Science of Remote Sensing 12 (2025) 100268

Contents lists available at ScienceDirect

Science of Remote Sensing

journal homepage: www.sciencedirect.com/journal/science-of-remote-sensing

Kernel density change: A new bitemporal lidar metric for directly mapping wildland fire fuel consumption

Michael J. Campbell [a,*], Andrew T. Hudak [b], T. Ryan McCarley [c], Benjamin C. Bright [b], Philip E. Dennison [a]

[a] School of Environment, Society and Sustainability, University of Utah, Salt Lake City, UT, 84112, USA
[b] Rocky Mountain Research Station, USDA Forest Service, Moscow, ID, 83843, USA
[c] American Forests, Washington, DC, 20005, USA

A R T I C L E I N F O

Keywords:
Lidar
Landsat
Fire ecology
Fire effects
Random forests
Aboveground biomass
Fuel consumption

A B S T R A C T

Biomass consumed in fires has direct ties to the carbon cycle and atmospheric emissions. Though pre- and post-fire aboveground fuel biomass can be estimated using ground measurements, scaling of fuel load and consumption estimates requires remote sensing. Increased availability of pre- and post-fire airborne lidar scans is enabling the spatially explicit quantification of fuel load changes. The most commonly applied multitemporal lidar-based fuel consumption mapping method is modeled fuel load change (MFLC), an indirect approach that differences separately modeled pre- and post-fire fuel loads to estimate consumption. In this study, we compared MFLC to a new modeling approach that directly predicts consumption from a suite of bitemporal point cloud structural change metrics. Kernel density change (KDC) quantifies pre-fire to post-fire change in Gaussian kernel point density at a series of aboveground heights. The fundamental assumption of KDC is that relative point density at a particular height corresponds to the amount of fuel at that same height; thus, the fire-induced change in this density should correspond to fuel consumption. Indeed, we found KDC outperformed the MFLC approach in predicting consumption across a diverse array of fuelbeds, from ground to canopy fuels. We also examined the degree to which adding Landsat time series data to the suite of lidar-based predictor variables could improve consumption models, finding that KDC saw substantial benefits from Landsat's inclusion whereas MFLC demonstrated little change. Our results suggest that KDC is a valuable method that could be employed where accurate maps of fuel consumption are needed.

1. Introduction

Accurate, spatially explicit quantification of wildland fire fuel consumption benefits our understanding of fire behavior, the types and amounts of emissions produced from fire, and the role that fire plays in the global carbon cycle (Larkin et al., 2014; Ottmar, 2014; Price et al., 2022; Restaino and Peterson, 2013). Fire behavior is driven by fuel load (i.e., live and dead biomass), fuel moisture, topography, and weather (Ottmar, 2014). Particularly in the presence of steep terrain and favorable weather conditions, more intense fires can yield higher rates of spread and flame lengths, both of which can inhibit wildland firefighters' suppression abilities and pose safety risks (Butler, 2014; Gallacher et al., 2018; Page and Butler, 2017). Fuel load directly constrains fire behavior based on availability of combustible material (Finney, 2001; Ottmar, 2014), with higher rates of fuel consumption (i.e., amount of live and dead biomass consumed during a fire) being proportionate to higher fire radiative power release and fireline intensities (Clark et al., 2020; Hudak et al., 2015; Wooster et al., 2021). Fuel consumption can serve as a direct proxy for fire emissions, improving our ability to understand land-atmospheric interactions and predict emission properties such as hazardous pollutant concentrations and their effects on respiratory health (French and Hudak, 2023) and microbial aerosolization and transport (Kobziar et al., 2018, 2024). Furthermore, quantifying fuel consumption within different fuelbeds – subsets of fuels grouped together based on shared structural characteristics, constituent materials, and associated fire behavior and effects – provides additional insight into the types and quantities of emissions produced from wildland fire (Riccardi et al., 2007; Weise and Wright, 2014). From a global carbon cycling perspective, fuel consumption represents the direct release of carbon stored in vegetation biomass – the

* Corresponding author. 260 South Central Campus Drive, Room 4625, Salt Lake City, UT, 84112, USA.
E-mail address: mickey.campbell@ess.utah.edu (M.J. Campbell).

https://doi.org/10.1016/j.srs.2025.100268
Received 12 March 2025; Received in revised form 10 July 2025; Accepted 4 August 2025
Available online 6 August 2025

conversion of a carbon sink into a carbon source (Loehman et al., 2014). Maps of fuel consumption, therefore, can meaningfully quantify and reduce uncertainty in the global carbon budget (Bright et al., 2022; French et al., 2004; Prichard et al., 2019a).

For decades, satellite time series data have been used to link spectral change to burn severity – an integrated measure of fire effects on vegetation and soil (Keeley, 2009; Morgan et al., 2014). Maps of burn severity are undoubtedly useful for post-fire land management, such as mitigating potential debris flows (Staley et al., 2018), planning revegetation operations (Morgan et al., 2015), and tracking ecosystem response (Bright et al., 2019; Lentile et al., 2007). Although the categorical nature of burn severity maps (i.e., "low", "moderate", or "high" severity) facilitates broad use, it also limits their utility in situations where quantitative measures of fire effects are needed. Furthermore, the lack of across-ecosystem transferability of burn severity ratings points to a need for a more consistent and less subjective approach to mapping fire's impacts (Kolden et al., 2015). Fuel consumption is an objective, transferable, and quantitative measure of the effect that fire has on a landscape, making it a more robust and precise metric than burn severity. However, changes in passive, optical spectral response may not be able to directly map fuel consumption, given the need to characterize structural changes to fuel loads in three dimensions (Garcia et al., 2017).

Lidar offers a viable solution to fuel consumption mapping, given its ability to precisely map three-dimensional fuel structure (Hudak et al., 2009). Studies have repeatedly demonstrated success in lidar-based modeling and mapping of fuel loads in different strata, ranging from ground fuels to surface fuels to canopy fuels (Engelstad et al., 2019; Kramer et al., 2016; Mutlu et al., 2008). Terrestrial and mobile lidar offer extreme precision, and have been frequently shown to be effective at mapping fuel loads, albeit only at local scales (Wallace et al., 2022). On the opposite extreme, spaceborne lidar such as the Global Ecosystem Dynamics Investigation (GEDI) could yield near-global estimates of fuel structure, albeit with comparably low accuracy and only in discrete, footprint-scale samples (Dubayah et al., 2020; Leite et al., 2022). Airborne lidar strikes a useful balance between three-dimensional structural detail and relatively large, spatially-exhaustive scans, offering the best solution for local-to-regional-scale fuel load mapping (Price and Gordon, 2016). A key challenge with airborne lidar-based fuel consumption mapping is the relative paucity of multitemporal data – a requirement for robustly evaluating load change over time in spatially coincident areas. As airborne lidar data availability has vastly increased in the US in the last decade, and as unoccupied aerial systems (UAS) use has proliferated during that same time, multitemporal lidar is becoming increasingly common, offering great potential for future fuel consumption mapping efforts (Okyay et al., 2019). In particular, fires that burn through existing airborne lidar coverage provide opportunities where only post-fire lidar collections are required to derive consumption estimates.

Most existing attempts to map fuel consumption using lidar have relied on an indirect approach that involves separately mapping pre- and post-fire fuel loads, and then differencing the two to yield consumption (or accumulation) estimates (Bright et al., 2022; Hudak et al., 2020; McCarley et al., 2020, 2024). Although demonstrated to be effective in several studies, the potential weakness of this approach lies in the propagation of uncertainty. Per-pixel uncertainty in pre-fire loads compounds with per-pixel uncertainty in post-fire loads, yielding higher levels of uncertainty in the resulting consumption predictions (Zhang et al., 2009). Inferences are further complicated when changes to fuel loads from other disturbances besides the fire are captured between the pre- and post-fire lidar collections, especially if scanned several years apart (McCarley et al., 2022).

An alternative approach would be to directly map fuel consumption – that is, constructing a predictive model in which the response variable is the fuel load change itself. This is fundamentally the approach that is taken in the passive optical mapping of burn severity, where differences in the normalized burn ratio before and after a fire serve as the basis of severity mapping (Eidenshink et al., 2007; Roy et al., 2021). Direct, lidar-driven approaches to mapping vegetation structural change have been developed, with some studies finding improved performance over indirect approaches and others finding the opposite, though none have been applied specifically in the context of wildland fire fuel consumption (Bollandsås et al., 2013; Cao et al., 2016; Dalponte et al., 2019; Loh et al., 2022; McRoberts et al., 2015; Zhao et al., 2018). One fire-focused example of direct, bitemporal change mapping is profile area change, which compares the area under the curve of lidar point height quantiles before and after a fire (Hu et al., 2019; Ma et al., 2018; Su et al., 2016). PAC has been shown to be effective at mapping burn severity but may struggle to quantify fuel consumption in different fuelbeds, given their height specificity.

In this study, we compared direct and indirect approaches for mapping fuel consumption in a series of recent prescribed fires in central Utah, USA. We used bitemporal airborne lidar data (2016 and 2023), along with field measurements of pre- and post-fire fuel structure, to evaluate and compare predictive model performance in a series of different fuelbeds. We also tested the extent to which the addition of Landsat-derived predictor variables could improve consumption predictions. In the course of this work, we developed a new, direct fuel consumption modeling approach – kernel density change (KDC) – that provides a normalized measure of point density change throughout the vertical fuel profile. We demonstrated that this direct mapping approach yielded substantially better model performance than the more common, indirect approach. Our results provide a robust, quantitative basis upon which future fuel consumption mapping efforts can be built, with a thorough evaluation of the strengths and weaknesses of direct and indirect consumption mapping techniques.

2. Methods

2.1. Study area

This study took place within the Monroe Mountain unit of the Fishlake National Forest in Utah, USA (Fig. 1A). It was chosen for the availability of both pre- and post-fire lidar and associated fuel plot data, as well as its extensive recent history of prescribed fires with high consumption totals. Monroe Mountain is one of the focal study areas of the Fire and Smoke Model Evaluation Experiment (FASMEE), giving it a rich scientific history that has produced a host of useful, fire-focused spatial data, some of which we rely on this study (Eagle et al., 2024; Prichard et al., 2019b). Centered at approximately 38.5817° N, 112.0147° W, this US Department of Agriculture (USDA) Forest Service-managed land encompasses a total area of approximately 711 km^2. Being situated in the moisture-limited Intermountain West region of the USA, the study area's wide elevation range (1707–3420 m) drives a large precipitation gradient, with lower elevations receiving <300 mm of precipitation annually and higher elevations receiving >800 mm annually, according to PRISM 30-year averages (1991–2020) (Daly et al., 1997). This environmental gradient, along with the area's extensive disturbance history due to fire and management, yields a spatially complex mosaic of vegetation type dominance. According to LANDFIRE, the most abundant vegetation types within Monroe Mountain are piñon-juniper woodland (27 % in 2016, representing the pre-fire conditions examined in this study; 24 % in 2023, representing the post-fire conditions), big sagebrush shrubland and steppe (2016: 17 %; 2023: 22 %), spruce-fir forest and woodland (2016: 12 %; 2023: 11 %), aspen-mixed conifer forest and woodland (2016: 12 %; 2023: 11 %); aspen forest, woodland, and parkland (2016: 8 %; 2023: 7 %), and Douglas-fir – Ponderosa pine – lodgepole pine forest and woodland (2016: 6 %; 2023: 5 %). Within the fuel plot data, which represent a small sample of the entire study area and are described in the next section, the following pre-fire vegetation types were represented: aspen-mixed conifer forest and woodland (50 % of plots), spruce-fir forest and woodland (37 %), aspen forest, woodland, and parkland

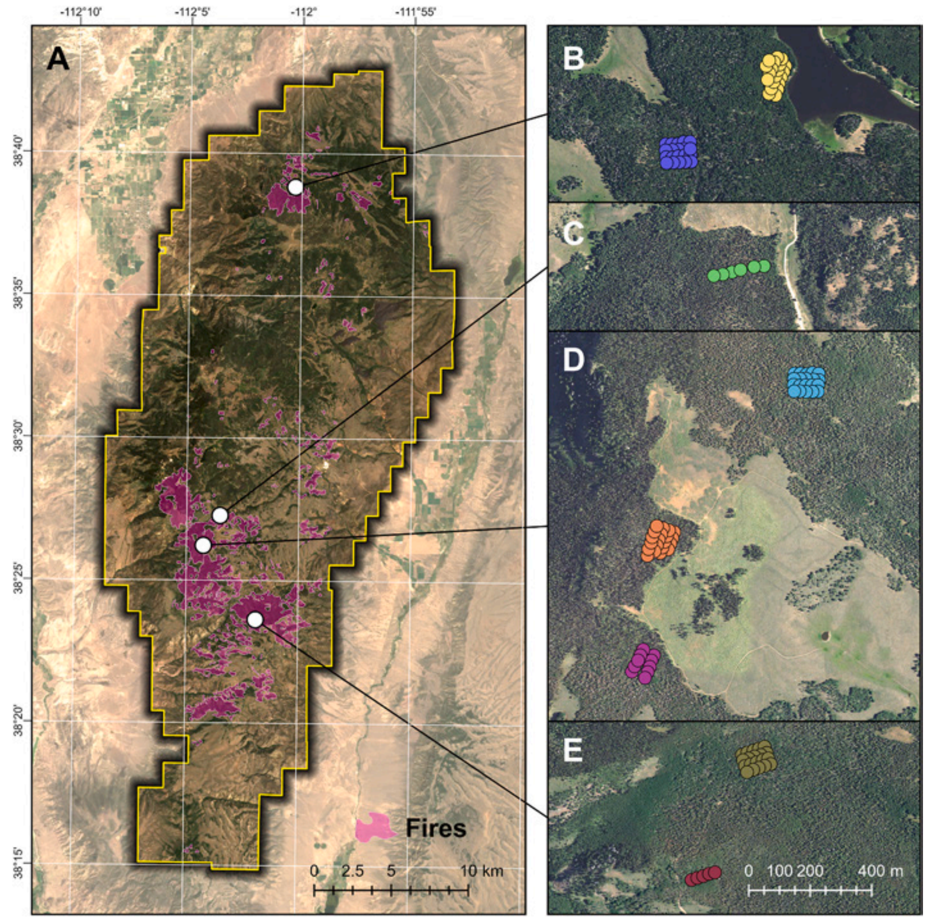

Fig. 1. Study area map featuring (A) the entire Monroe Mountain unit of the Fishlake National Forest and (B–E) larger-scale focus maps that highlight the field plots within which fuel measurements were collected, colored by the clusters that were used for spatial cross-validation. The background images shown are from (A) Landsat 8, and (B) the National Agricultural Inventory Program, both captured in 2016, representing pre-fire conditions. The 121 plot locations in (B–E) are plot center points, enlarged for enhanced visibility and do not represent true plot dimensions. The fire perimeters are approximated and derived from thresholding of Landsat normalized burn ratio differences between successive years within the time frame (2016–2023).

(11 %), and western riparian woodland and shrubland (2 %).

2.2. Field data

To serve as the basis of fuel consumption model training and validation, we used a database of fuel plot data (Fig. 1B–E) (Eagle et al., 2024). Collected between 2016 and 2021 by the Fire and Environmental Research Applications team of the USDA Forest Service, the database contains 121 plot locations where fuel load measurements were acquired before and after a series of prescribed fires in the study area, i.e., a field crew visited each of the 121 plots twice, both before and after burning. The plots were laid out in grid patterns with at least 20 m spacing between plots, clustered into eight groups. As discussed later in Section 2.6, this between-plot proximity and clustering could result in a significant effect of spatial autocorrelation, which we address through a strategic, cluster-based cross-validation procedure.

The fuel plot layout can be seen in Fig. 2. As described in Eagle et al. (2024), these fuels were measured using a combination of direct (i.e., clipping, drying, and weighing) and indirect (i.e., allometric) methods. Fine woody debris (1-h and 10-h), herbs, shrubs, and seedlings were measured directly in small (either 0.25 m^2 or 1 m^2) clip plots. One clip plot was measured before the fire and a separate clip plot was measured after the fire, since clipping removed the fuels prevented remeasurement in the same location. Duff, litter, lichen, and moss fuel loads were estimated indirectly using eight depth measurements in a dedicated subplot that was spatially separated from the main plot, with loads computed using allometric bulk densities from Prichard et al. (2017). Coarse woody debris (100-h and 1000-h) was measured indirectly using three 10 m transects radiating out from plot center separated by 120° with a random starting azimuth and allometric equations from Brown et al. (1982). Mature trees – those taller than breast height with a stem diameter at breast height greater than 12 cm, where breast height is 1.37 m – were measured for their stem diameter within an 8 m-radius circular plot area. Saplings – those taller than breast height with a stem diameter less than 12 cm – were tallied within a 5.6 m-radius circular plot area. Allometric tree fuel loads for mature trees and saplings were derived using the Fire and Fuels Extension of the Forest Vegetation Simulator (Reinhardt and Crookston, 2003).

From the field data, we calculated fuel loads in 16 different fuelbeds, some of which are aggregated from others, and each of which served as the response variable for our machine learning models (Table 1). Tree fuels were only measured on approximately half (n = 61) of the plots, so for each fuelbed, only those plots with relevant measurements were included in the modeling process. All fuel load and consumption totals discussed throughout this study are measured in megagrams per hectare ($Mg \cdot ha^{-1}$). Note that we did remove one outlier plot from consideration as it featured an implausible, nearly 500 % increase in 1000-h fuels post-fire (likely caused by a falling snag from the fire), whereas all other plots (n = 120) saw either minor increases or, dominantly, large decreases in woody debris due to consumption.

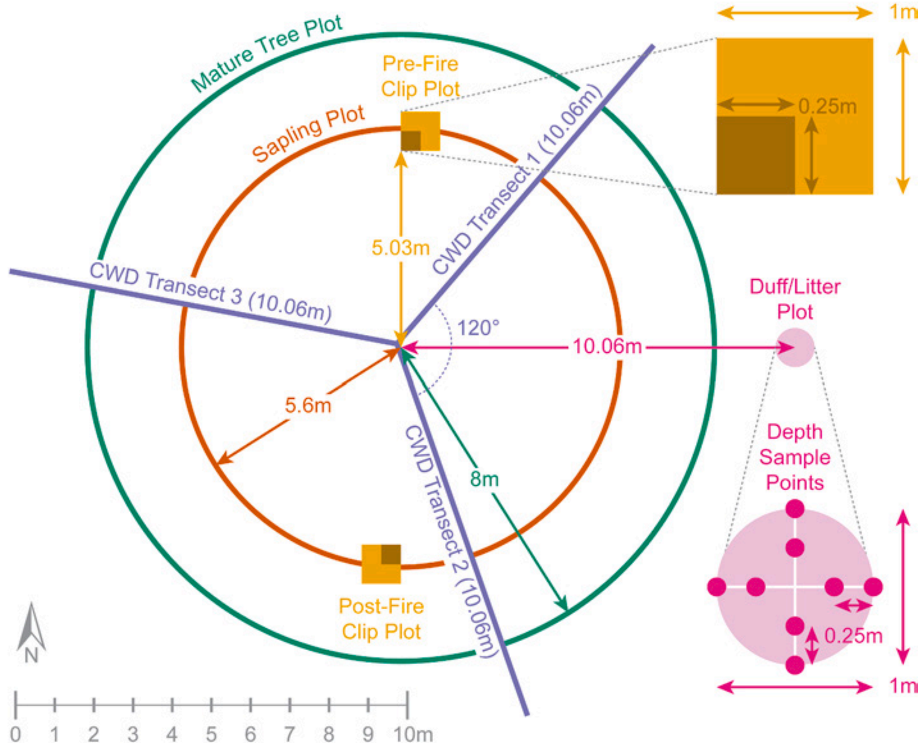

Fig. 2. Field plot layout.

Table 1
Fuelbeds directly measured and aggregated from the field data, for which we modeled consumption in this study. The fuelbed numbers are not formal designations but are provided for convenience in describing aggregated fuelbeds.

Fuelbed Number	Fuelbed Component	Description
1	1-Hour	Fine dead surface woody debris fuels whose particles are <0.64 cm in diameter
2	10-Hour	Fine dead surface woody debris fuel whose particles are 0.64–2.54 cm in diameter
3	100-Hour	Coarse dead surface woody debris fuel whose particles are 2.54–7.62 cm in diameter
4	1000-Hour	Coarse dead surface woody debris fuel whose particles are >7.62 cm in diameter
5	Woody Debris	All downed woody debris – the sum of fuelbeds 1, 2, 3, and 4
6	Duff	Ground fuels comprising the organic matter (partially or fully decomposed wood, leaves, twigs, etc.) that sits atop the mineral soil surface
7	Litter, Lichen, Moss	Dead surface fuels comprising leaf litter, lichens, and mosses
8	Herb	Live herbaceous (non-woody) surface fuels comprising grasses and forbs
9	Shrub	Live shrubby surface fuels comprising all woody plants not classified as trees
10	Seedling	Live tree fuels for trees <1.37 m in height
11	Shrub + Seedling	Low-stature live surface fuels – the sum of fuelbeds 9 and 10
12	Non-Tree	All non-tree fuels – the sum of fuelbeds 5, 6, 7, 8, and 11
13	Tree	All tree fuels, including all live and dead standing boles, branches, and foliage
14	Available Canopy	Fine tree branch and foliage fuels
15	Total	All fuel combined – the sum of fuelbeds 12 and 13
16	Available	All fuels most readily available for consumption – the sum of fuelbeds 12 and 14

2.3. Lidar data

Two airborne lidar datasets were used in this study, one collected in 2016, representing pre-fire conditions, and one from 2023, representing post-fire conditions. The 2016 data were flown between August 3rd and October 12th, with an average pulse density of 12.9 pulses/m^2 after pre-processing. The 2023 data were flown between September 19th and September 23rd, with an average pulse density of 19.3 pulses/m^2 after pre-processing. All lidar data were processed using a combination of *LAStools* and the *lidR* library in *R* (Isenburg, 2015; R Core Team, 2021; Roussel et al., 2020). Lidar data pre-processing proceeded as follows. First, points classified as noise or flagged as withheld were removed from the datasets. Next, points classified as “overage” – falling within the overlap between two or more flight line scan areas – were removed, to minimize the influence of high scan angle points on structural estimates and minimize scan line artifacts (Price and Gordon, 2016; Yan, 2023; Zaragosa et al., 2016). This was accomplished using the *lasoverage* function in *LAStools* (Isenburg, 2015). Lastly, point heights were converted from raw elevations to aboveground heights by per-point subtraction of a terrain model, which was created through triangulated irregular network-based interpolation of ground-classified points. All points with aboveground heights greater than 50 m were removed, as no vegetation in this study area reaches such heights. All points with heights less than −1 m were also removed, as these likely represented noise that was not captured during noise removal. Remaining negative-height points were coerced to a height of zero, as these likely reflected small uncertainties in the ground point classification process.

For use in modeling and mapping of fuel consumption, the lidar data were used to generate predictor variables in two different ways. To build and validate models, predictor variables were computed at the plot level, using point clouds clipped to the extent of an 8 m radius circle around each plot center, encompassing the largest dimension of measured fuels in each field plot. To map fuel consumption across the entire study area (i.e., to apply the models for prediction purposes), predictor variables were computed at the pixel level, with a spatial resolution of 15 m to approximately match the area of the fuel plots. The specific predictor variables are described in Sections 2.4.1 and 2.4.2.

2.4. Fuel consumption model types

A summary of the two fuel consumption model types tested in this study can be seen in Fig. 3: fuel load change (MFLC; described in detail in Section 2.4.1) and kernel density change (KDC; Section 2.4.2). Briefly, MFLC is an indirect fuel consumption modeling approach that relies on the change between separately modeled pre- and post-fire fuel loads. KDC is a direct fuel consumption modeling approach, where fuel load change is directly modeled, that relies on the pre-/post-fire differences in kernel density estimates of lidar points at a series of heights. For both models, we also tested the effect that including Landsat image data had on model performance (Section 2.5). The modeling procedure is described in Section 2.6.

2.4.1. Modeled fuel load change (MFLC)

MFLC entails making two sets of model predictions, one representing pre-fire fuel loads and the other representing post-fire fuel loads. To map consumption, post-fire predictions are subtracted from pre-fire predictions. In this sense, MFLC is considered an indirect fuel consumption mapping approach, as consumption is a secondary product derived from two directly modeled sets of predictions. McCarley et al. (2020) described two different MFLC approaches. The first involves creating two separate models, one for pre-fire fuel loads and one for post-fire fuel loads. In this scenario, pre-fire fuel plot data train and validate a predictive model with a suite of predictor variables derived from pre-fire lidar data. Separately, post-fire fuel plot data train and validate another predictive model with post-fire lidar predictors. Henceforth, this model architecture will be referred to in this study as "MLFC Pre-Post". The second approach described by McCarley et al. (2020) creates a single model by combining (pooling) pre- and post-fire fuel plot and

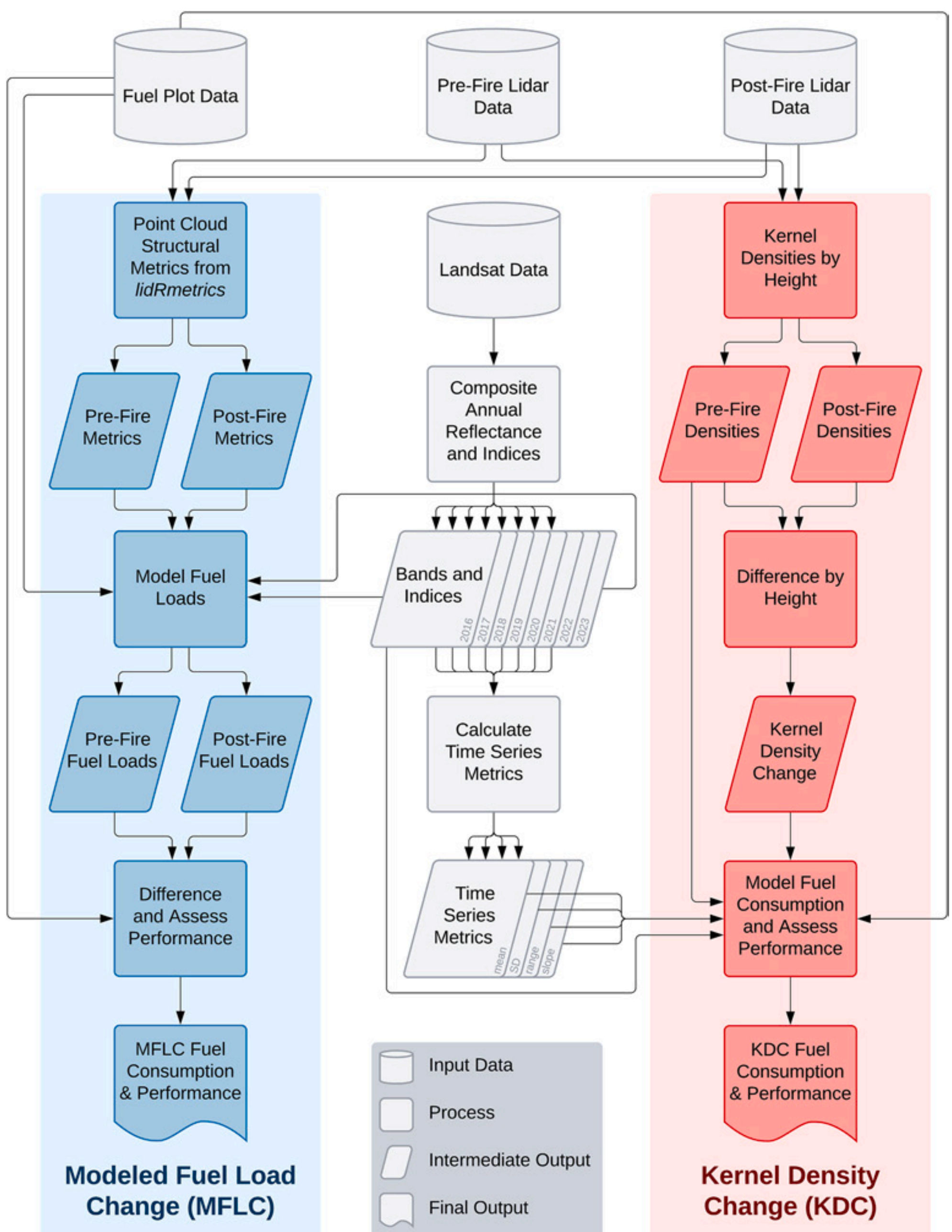

Fig. 3. Workflow summary for the two different fuel consumption model types performed and compared in this study.

lidar data. In effect, this doubles sample size, can potentially help minimize the confluence of uncertainty arising from modeling pre- and post-fire fuels completely separately, and captures a wider range of forest conditions (unburned to high consumption) in a single model. Hereafter, this model type will be referred to as "MFLC Pooled".

We tested both of these approaches in this study. An important consideration in either approach is the identification of a useful set of lidar predictor variables that should capture variance in fuel loads in different fuelbeds, from ground to canopy. To that end, we opted to employ the *lidRmetrics* library in R, which has adeptly aggregated a diverse suite of vegetation structural metrics to support modeling efforts such as this study (Tompalski, 2023). We used the *metrics_set3()* function to derive the most comprehensive set of predictors offered by the library. We removed a subset of variables that were point density-dependent and based on raw (rather than relative) quantities (e.g., number of points, number of first returns, etc.), as they would not readily scale between different spatial units (e.g., plot circles versus map pixels) or lidar datasets (e.g., lower-density 2016 data versus higher-density 2023 data). We also removed any variables that yielded NA values within any of the fuel plots, as they would negatively affect our model construction. In total, this yielded a set of 85 predictor variables. For a complete description of the variables and the code used to generate them, we refer readers to https://github.com/ptompalski/lidRmetrics.

2.4.2. Kernel density change (KDC)

To test the degree to which consumption in different fuelbeds could be modeled directly – that is, where consumption, itself, is the model's response variable – we devised a new metric called kernel density change (KDC) (Fig. 4). The underlying assumption of KDC is that changes in fuel loads will be captured by changes in the distribution of lidar points before and after a fire. Driven by a Gaussian kernel density estimator with a defined bandwidth, lidar point densities are computed from pre- and post-fire lidar at a defined interval of vertical heights, from the ground to the top of the canopy. By subtracting post-fire densities from pre-fire densities, the change is quantified at each height individually.

In our study, we defined the bandwidth to be 5 cm (Fig. 5). This is equivalent to the standard deviation of the Gaussian kernel applied to each point. In effect, this means that relative point densities at each height of interest are calculated based not on the binary presence/absence of a point within a defined bin, but instead on the assumption that each point return possess its own Gaussian height distribution, 99 % of which falls within a ±15 cm range of its recorded height. In this way, we account for the vertical uncertainty in a lidar point return's z coordinate. We defined the vertical height interval to be 10 cm, such that for

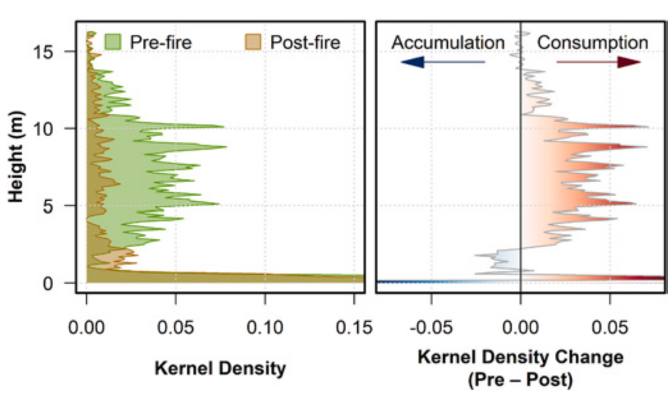

Fig. 4. An illustrative example of kernel density change. The left plot shows lidar point kernel density distributions by height for the same location before and after a fire. The right plot shows the difference between the two, with higher positive values being representative of fuel consumption and lower negative values being representative of fuel accumulation.

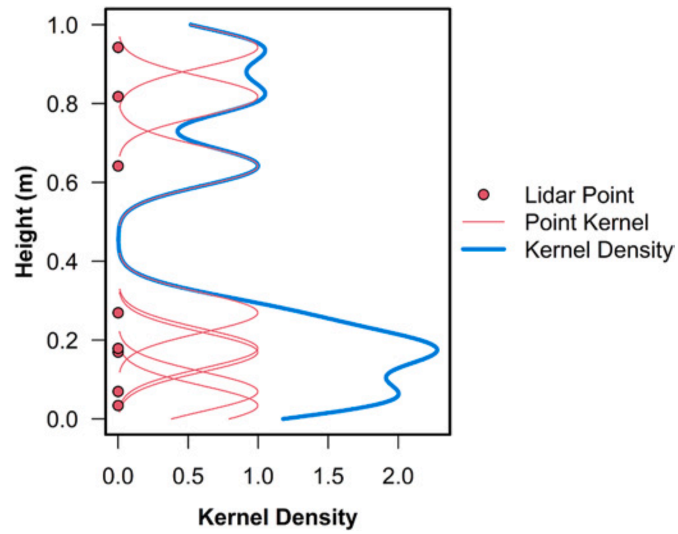

Fig. 5. Example of how Gaussian kernel density is calculated for eight artificial lidar points between 0 and 1 m in aboveground height. Each point is given its own Gaussian kernel, with a bandwidth (i.e., standard deviation) of 5 cm. The combined kernel density is then calculated as the sum of the individual point kernel densities, normalized so that the area under the entire curve sums to 1.

every 10 cm from the ground to the top of the canopy (the maximum of which we defined to be 20 m), we computed kernel density. The integral of a kernel density function is always equal to one, which ensures direct comparability between lidar datasets (and subsets thereof) with differing raw point densities. We did not distinguish between ground and non-ground points in kernel density calculations, as increased densities in ground points post-fire could suggest higher fuel consumption totals. In all, this yielded 201 candidate predictor variables for KDC-based mapping of fuel consumption.

We devised two types of KDC models. The first included only the 201 KDC variables previously described, representing lidar point density change at a series of heights. This model type will be referred to as "KDC Diff Only", as only differences in point density are included as predictors. In recognition of the fact that pre-fire fuel structure may inform consumption, we created a second type of model that included the 201 pre-fire height kernel density estimates along with the 201 KDC variables. The assumption here is that knowing how much fuel is in a plot or pixel before the fire may provide useful predictive context for the KDC variables' quantification of height-specific change. This model type will be referred to as "KDC Pre and Diff".

2.5. Landsat data

To evaluate the potentially useful role that spectral data could play in addition to lidar, we acquired a time series of Landsat data (Fig. 3). Using Google Earth Engine, we generated annual summer median cloud-free, snow-free Landsat 8/9 surface reflectance composites using the Collection 2, Tier 1, Level 2 data (Crawford et al., 2023; Gorelick et al., 2017). We generated one image per year from 2016 to 2023 to match the date range of the lidar data. Using the raw spectral data in each image, we derived a suite of spectral indices, including the normalized difference vegetation index (NDVI), enhanced vegetation index (EVI), soil adjusted vegetation index (SAVI), modified soil adjusted vegetation index (MSAVI), normalized difference wetness index (NDWI), normalized burn ratio (NBR), normalized burn ratio 2 (NBR2), and the near infrared reflectance of vegetation (NIRv). To capture change over time, we computed a series of per-pixel temporal metrics that leveraged the full eight-year time series. For all of the aforementioned indices, as well as raw surface reflectance for each of Landsat's seven visible – shortwave infrared bands, we generated the following time series metrics: mean, range, standard deviation, and regression line slope. We selected these metrics with the intent to capture the presence/absence, relative consumption, and timing of fire (Figure A1). The Landsat data were down-sampled to 15 m resolution, to match the lidar-derived predictors, as all predictor variables needed to exist on the same pixel grid. This was done using bilinear interpolation. All image processing was done using the *terra* library in *R* (Hijmans et al., 2023).

To test Landsat's potential value in modeling fuel consumption, for each of the two model types described earlier (MFLC and KDC), the models were run with and without Landsat data. For the MFLC models, 2016 and 2023 Landsat surface reflectance and spectral indices were used to capture pre- and post-fire spectral conditions. For the KDC models, the change in aforementioned spectral change metrics (mean, range, standard deviation, and trendline slope) were used to capture fire-induced changes in spectral conditions. Recall that a subset of the KDC models also included pre-fire lidar structure as candidate predictors. To mirror this concept, for KDC Pre & Diff models, 2016 Landsat surface reflectance and spectral indices were also added to the pool of potential predictor variables.

2.6. Modeling

In all, eight model types were evaluated in this study (Table 2). Each of these eight model types was applied to each of the 16 fuelbeds of interest, yielding 128 separate models. To ensure that models were being compared in an equitable manner, the same modeling workflow was applied for each, as follows. Random forests were used as the predictive algorithm, as implemented in the *ranger* package in *R*, given their ability to handle large numbers of predictor variables, robustness against multicollinearity, and reliable quantification of variable importance (Breiman, 2001; Wright and Ziegler, 2017). In each model, a series of tuning steps were performed, using the entire fuel plot dataset as training. First, to distill the large pool of candidate predictor variables down to a parsimonious, meaningful, and maximally predictive set, we used the variable selection using random forests (VSURF) algorithm (Genuer et al., 2015). We used this refined set of predictors to tune some of random forests' most important hyperparameters. These included *mtry* (the number of variables tested at each decision tree split), *min.node.size* (the smallest number of training points allowed in a decision tree's terminal node), and *sample.fraction* (the proportion of training data sampled for each decision tree's construction). A random search grid of 100 hyperparameter combinations was tested, and the combination with the lowest out-of-bag error was selected for model construction (Bergstra and Bengio, 2012).

As seen in Fig. 1, the field data are highly clustered in space. Failing to account for this clustering could yield an inflated sense of model performance, as spatial autocorrelation could be responsible for artificially increasing the apparent accuracy of predictions (Ploton et al., 2020). Accordingly, we devised a robust model performance assessment approach that employed a spatial cross-validation technique that should be a better representation of model performance if applied to prediction in a different geographic location. There were eight clusters of plots (Fig. 1). To evaluate model performance, each of these plot clusters was iteratively set aside as a validation dataset, with the remaining seven being used to construct a variable-selected and hyperparameter-tuned model. Predictions were made on each fold, the compilation of which was compared to all observations. Performance was assessed according to R^2, which should capture the linear correlation between predictions and observations, and %RMSE, which should capture the proportional predictive error. %RMSE was calculated as the RMSE divided by the mean of observed values. Lastly, to build a singular model for making per-pixel spatial predictions (i.e., mapping fuel consumption) and assessing variable importance for each fuelbed, data from all plots were used. Variable importance was computed as the percent increase in mean squared prediction error that occurred when a predictor variable's values were randomly permuted.

Given the large number of models tested, each featuring a large set of candidate predictor variables, we devised a tailored approach to conveying variable importance in a distilled, aggregated manner. We focused our evaluation of variable importance on the four types of KDC models, given their comparable performative superiority. To understand what heights were most important predictors of consumption across the 16 focal fuelbeds, we computed average permutation importance of any kernel density-based predictor variable (i.e., pre-fire kernel density or KDC) that was selected in any of the KDC models. For example, if pre-fire kernel density at 1 m was selected and featured a permutation importance of 5 % in one model, KDC at 1 m was selected with an importance of 10 % in a second model, and no other 1 m-height kernel density predictors were selected in any other model, the mean importance would be 7.5 %. For the Landsat data, each spectral band or index had five potential predictor variables, including pre-fire data and four change metrics (mean, SD, range, slope). Among the models that

Table 2
Summary of the eight model types compared in this study, including the numbers of candidate predictor variables included in the construction of each model.

Indirect vs. Direct	Model Type	Model Description	Candidate Predictor Variable Sets					
			Pre-Fire Lidar Metrics	*Post-Fire Lidar Metrics*	*Lidar Change Metrics*	*Pre-Fire Landsat Metrics*	*Post-Fire Landsat Metrics*	*Landsat Change Metrics*
Indirect	MFLC Pre-Post: Lidar	Modeled fuel load change with separate models for pre- and post-fire fuel loads using only lidar data	85	85	–	–	–	–
Indirect	MFLC Pre-Post: Lidar + Landsat	Modeled fuel load change with separate models for pre- and post-fire fuel loads using lidar and Landsat data	85	85	–	15	15	–
Indirect	MFLC Pooled: Lidar	Modeled fuel load change with separate models for pre- and post-fire fuel loads using only lidar data	85	85	–	–	–	–
Indirect	MFLC Pooled: Lidar + Landsat	Modeled fuel load change with separate models for pre- and post-fire fuel loads using lidar and Landsat data	85	85	–	15	15	–
Direct	KDC Diff Only: Lidar	Kernel density change using only lidar data	–	–	201	–	–	–
Direct	KDC Diff Only: Lidar + Landsat	Kernel density change using lidar and Landsat data	–	–	201	15	–	60
Direct	KDC Pre & Diff: Lidar	Kernel density change with pre-fire densities using only lidar data	201	–	201	–	–	–
Direct	KDC Pre & Diff: Lidar + Landsat	Kernel density change with pre-fire densities and spectral data using lidar and Landsat	201	–	201	15	–	60

featured Landsat predictors, the average variable importance of any of those metrics that were selected was computed. For example, if pre-fire NDVI was selected with an importance of 20 % in one model, NDVI range was selected with an importance of 30 % in a second model, and no other NDVI-based metrics were selected in any other models, the mean importance would be 25 %.

Beyond importance, there is inherent value in understanding predictor-response relationships. To investigate these relationships, we divided plots into "high" and "low" consumption. "High" consumption plots were those that featured total fuel consumption greater than or equal to the median among all field plots. "Low" consumption plots were less than the median. To understand the relationship between KDC and consumption, we computed the medians and interquartile ranges of KDC values at each height (0–20 m, at 0.1 m interval) among "high" and "low" consumption plots. To understand the relationship between Landsat data and consumption, we computed the medians and interquartile ranges of Landsat variable ranges (i.e., the differences between the maximum and minimum band or index values in the time series) among "high" and "low" consumption plots.

We also tested a hybrid modeling approach that combined predictor variables from MFLC and KDC, the methodology and results for which can be found in Appendix B.

3. Results

3.1. Fuel consumption models

Among the lidar-only models, performance varied substantially by fuelbed and model type (Table 3; Fig. 6). Across model types, the fuelbeds that yielded the best models (highest R^2 and lowest %RMSE) were available canopy fuel and total tree fuel. Intermediate performers included 1000-h fuel, total woody debris, non-tree fuel, total fuel, and total available fuel. Poor performers included 1-h fuel, 10-h fuel, 100-h fuel, litter, lichen, and moss fuel, duff, shrub fuel, seedling fuel, shrub and seedling fuel, and herbaceous fuel. The overarching trends were: (1) models based on tree fuel consumption yielded the highest predictive power; (2) models with larger fuel particles and more aggregated fuel measures performed moderately well; and (3) models with smaller fuel particle with lower overall loads produced the poorest performance. The predicted versus observed scatterplots for all models tested in this study can be found in Figures A2-A9 in Appendix A. Of particular note among these figures is the relatively poor distributions of observed consumption values in herbaceous and shrub fuels. These distributions drove very high %RMSE values among these fuelbed models.

Across model types and fuelbeds, the vast majority of models yielded significantly ($p < 0.01$) non-zero regression slopes between predictions and observations, suggesting at least a minimum threshold of ability to predict consumption to a useful degree. Among the significant lidar-only models (Fig. 6A and B), KDC outperformed MFLC in most cases, with the exception of available fuel, total fuel, and available canopy fuel. This is particularly noteworthy, as MFLC approaches have been the dominant technique for fuel consumption mapping to date. These results point towards the fact that KDC's direct fuel modeling approach may be preferable to MFLC's indirect approach in fuel consumption mapping.

Including Landsat data offered a substantial performance boost to KDC models, with most demonstrating higher R^2 and lower %RMSE (Fig. 6C and D and 7). Indeed, the few aforementioned fuelbeds where MFLC outperformed KDC with lidar data alone saw a reversal of this outperformance when Landsat data were included. Landsat's inclusion had essentially no effect on the performance of the MFLC models. This suggests that, when mapping fuel loads at one or two points in time (i.e., with MFLC), spectral data do not offer much predictive information that the structural data from lidar do not already possess. Conversely, when mapping fuel consumption in a direct manner (i.e., with KDC), the spectral change metrics can help inform the models' ability to quantify the degree of landscape change caused by fire.

When viewing the lidar-only and lidar + Landsat results together by fuelbed, it becomes clear that KDC methods are superior in most cases, with the highest R^2 in 89 % of the significant models and lowest %RMSE in 90 % of models (Fig. 8). Within the KDC models, it appears that including pre-fire densities (i.e., KDC Pre & Diff) yields a noteworthy benefit in the majority of cases.

Table 3
Mean model performance by fuelbed among all four lidar-only models, including MFLC Pre-Post: Lidar, MFLC Pooled: Lidar, KDC Diff Only: Lidar, KDC Pre & Diff: Lidar (see Table 2 for model details).

Fuelbed Component	Mean R^2	Mean %RMSE
1-Hour	0.02	159
10-Hour	0.14	168
100-Hour	0.20	98
1000-Hour	0.45	66
Woody Debris	0.43	61
Duff	0.19	93
Litter, Lichen, Moss	0.15	70
Herb	0.00	4110
Shrub	−0.01	883
Seedling	0.11	153
Shrub + Seedling	0.07	152
Non-Tree	0.32	63
Tree	0.59	49
Available Canopy	0.60	37
Total	0.37	51
Available	0.30	62

3.2. KDC variable importance

We sought to better understand how KDC models were making predictions by inquiring into what variables were selected, their importance, and their relationship with the fuel consumption response variables (Fig. 9). Among the KDC variables (Fig. 9B), there appears to be a somewhat bimodal distribution of variable selection and importance by height, such that KDC metrics closer to ground level (<2.5 m in height) and KDC metrics near the top of the canopy (>15 m) were selected more frequently and were found to have higher importance. Comparing relatively high consumption versus relatively low consumption plots provides some insight into why this bimodal distribution emerged (Fig. 9D). Note that, since KDC represents the point density difference between pre- and post-fire lidar data, positive values are associated with consumption (higher pre-fire density minus lower post-fire density), and negative values are associated with accumulation (lower pre-fire density minus higher post-fire density). KDC values with a magnitude approaching zero should mean that little to no change occurred at a given height between the two time frames.

High-consumption plots featured greater positive KDC values (decrease in lidar point density over time) throughout most of the canopy (2.5–20 m) than low consumption plots. In the 1–2.5 m surface fuel range, high consumption plots featured greater negative KDC values (increase in density), which we attribute to regeneration of dense aspen that occurred in years between fires and the post-fire lidar scan. Indeed, one of the primary objectives of the prescribed fires in the study area is to promote aspen forests, which vigorously sprout in the wake of fire in this ecosystem (Kitchen et al., 2019). Though not directly visible in Fig. 9D, there are two other KDC trends worth noting. First, high consumption is associated with a spike in positive KDC just above ground level (0.2–1 m), which we attribute to consumption of low surface and ground fuels. Second, high consumption plots featured a strong negative KDC at 0 m in height, which we attribute to the greater proportion of lidar pulses reaching the ground in plots where much of the energy-absorbing aboveground fuel had been removed.

The importance of Landsat variables was generally quite high (Fig. 9A) – often, higher than KDC variables – which bolsters the previously described notion that Landsat played a valuable role in

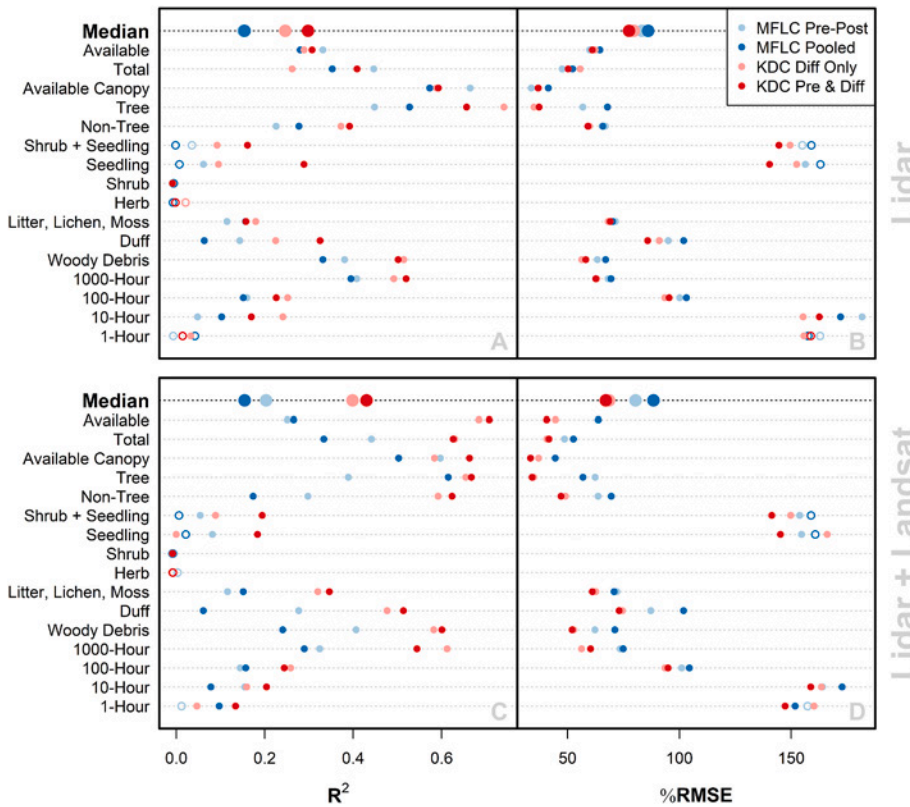

Fig. 6. Model performance by fuelbed (rows) and model type (point colors), according to R^2 (A and C) and %RMSE (B and D). The top row (A and B) represents the performance of models built only with lidar-based predictor variables, whereas the bottom row (C and D) represents the performance of models that included both lidar and Landsat predictor variables. Note that the range in %RMSE values shown excludes the high values for shrub and herb fuelbeds to improve visual clarity. Models with statistically significant ($p < 0.01$) regression slopes between predictions and observations are shown with filled circles, whereas non-significant models are shown with empty circles.

increasing fuel consumption predictive power. Among the four different types of Landsat time series metrics, range was selected most frequently (36 times), followed by standard deviation (23), slope (22), and mean (15). The shortwave infrared bands (B6 and B7) and indices (NBR and NBR2) were selected frequently, which aligns with this spectral region's historical value in mapping burn severity (Eidenshink et al., 2007; Key and Benson, 1999; Miller et al., 2009). Among these variables, the ranges for high consumption plots tended to be greater than those of low consumption plots, suggesting that the magnitude year-over-year changes in shortwave infrared reflectance is a valuable predictor of consumption (Fig. 9C). NDVI played an important role in quantifying fuel consumption in several fuelbeds, with a very clear separation between low and high consumption plots (Fig. 9A and C). The visible bands (B1 – B4) were selected and featured high importance in several models as well, though the difference between high and low consumption spectral ranges were quite low.

3.3. Fuel consumption maps

In spatial modeling studies such as this, solely focusing on the quantitative performance metrics in a non-spatial fashion (as is done in Section 3.1 above) fails to capture an important consideration of true predictive performance. The spatial dimensions of the fuel consumption maps also provide invaluable insight into the strengths and weaknesses of different model types applied to different fuelbeds. Although we generated maps for each fuelbed, for simplicity, we focus this section on total fuels, as it is both the most important measure of consumption that incorporates all others, and its spatial patterns are representative of mapped consumption in other fuelbeds (Fig. 10). Perhaps the most significant result that emerges from a visual comparison of the predicted outputs is the important role that Landsat image data played in reducing noise in the per-pixel consumption estimates. Across almost all model types, using lidar data alone yielded noisy predictions, with areas clearly outside of fire extents yielding sometimes relatively high consumption estimates. The one exception to this was the MFLC Pooled: Lidar model, which featured the clearest distinction between burned and unburned areas using lidar alone. Although KDC had the highest quantitative model performance of the three model types, in the absence of Landsat data, its predictive maps appear to contain the most noise, at least for total fuels. However, with the help of Landsat, the two KDC-based maps (KDC Diff Only: Lidar and KDC Pre & Diff: Lidar + Landsat) featured a clearer spatial distinction between burned and unburned areas.

4. Discussion

In this study, we compared two methods for fuel consumption mapping: MFLC and KDC. MFLC is an indirect change mapping approach that relies on the differences between fuel load predictions made pre- and post-fire. Conversely, KDC is a direct change mapping method, where fuel consumption is modeled as a function of lidar structural change metrics. Comparisons between direct and indirect methods have been made previously, albeit in a non-wildland fire context, with some studies finding direct methods to be superior (e.g., Bollandsås et al., 2013; Cao et al., 2016) and others arriving at opposing conclusions (e.g., Loh et al., 2022; McRoberts et al., 2015). MFLC has been applied most frequently to fuel consumption mapping efforts in the past; however, in this study we found it to be generally worse than KDC. KDC is an entirely new metric introduced in this study for mapping fuel consumption. It provides a valuable methodological contribution to the remote sensing and fire ecological disciplines, as future studies in these arenas may

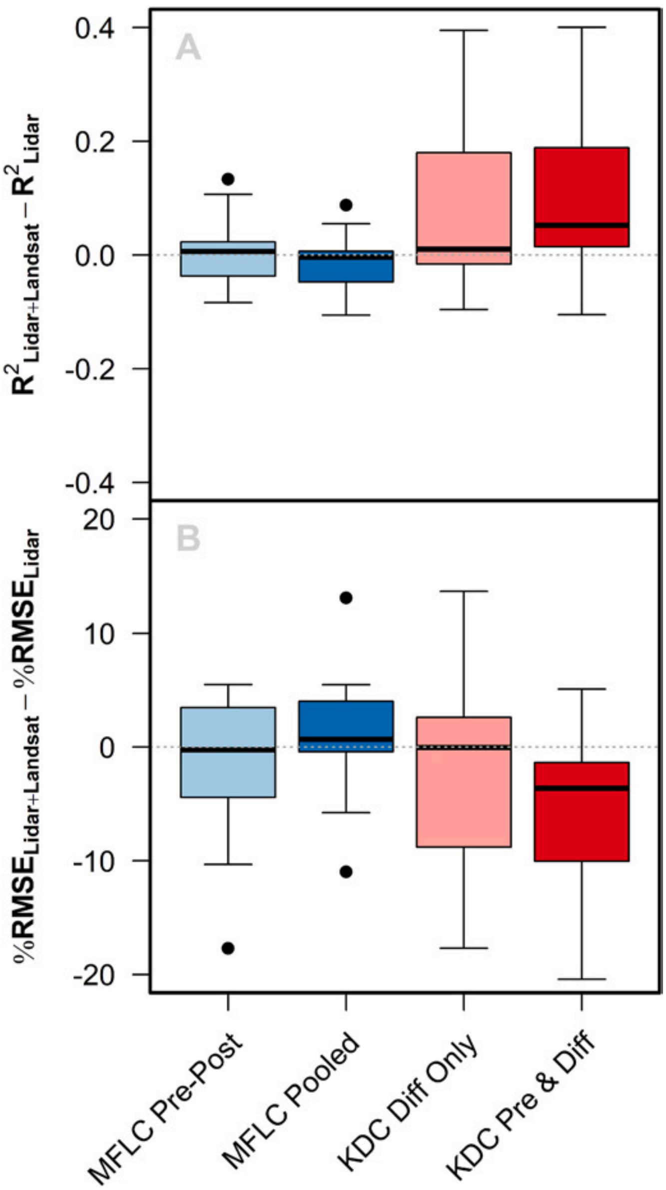

Fig. 7. Change in model performance with the inclusion of Landsat data, according to R^2 (A) and %RMSE (B). In both cases, the gray, dashed, horizontal line at zero represents no model performance change. In (A), distributions falling above that line represent improved performance with the inclusion of Landsat data. In (B), distributions below the line represent improved performance.

benefit from its ability to accurately predict change in fuel loads in a diverse range of fuelbeds. Our KDC method could also potentially be applied to quantify vegetation changes caused by other disturbance agents, such as insects (Campbell et al., 2024; Meng et al., 2018), drought (Brodrick and Asner, 2017; Campbell et al., 2020), timber harvesting (Fisher et al., 2024), and windthrow (Einzmann et al., 2017).

Although MFLC performed the worst of the two methods, it does possess a few unique benefits not provided by the two direct change mapping approaches. First, by its very nature, MFLC produces three maps: (1) pre-fire fuel loads; (2) post-fire fuel loads; and (3) fuel consumption. Although the focus of this paper has been on the degree to which (3) could be accurately predicted, there is great value in having (1) and (2) as byproducts. Fuel load maps are inherently valuable for a range of applications, including fire behavior modeling, estimating emissions, prioritizing fuel treatments, and understanding wildfire risk. A second benefit of MFLC – at least the pooled version – is the fact that even without the support of Landsat data, it did not widely predict fuel consumption outside of known burn areas, which both of the lidar-only direct methods did. A third benefit, and perhaps why it has been most used to estimate and map fuel consumption, is that it does not rely upon field observations of fuel consumption. That is, field observations of fuels can be taken pre- or post-fire at different locations, potentially even outside fire extents, although doing so prevents direct quantification of fuel consumption prediction accuracy. Conversely, our direct KDC method relies upon paired field observations of fuel consumption, where pre- and post-fire fuels are measured at the same locations. Thus, applying these direct approaches depends upon (1) a sample of pre-fire fuel observations being available within fire extents and (2) the ability to resample fuels at these same locations post-fire. Such data are likely to be only available within prescribed fires, given advance knowledge of where fires are going to occur. However, with a sufficiently representative set of fuel consumption field measurements and associated lidar data, existing models could be applied to new lidar acquisitions as well, with the understanding that predictive uncertainties may be higher when applied beyond the pyrogeographical context of the data on which the models were trained.

Spectral data, in this case derived from a time series of Landsat imagery, played an important but algorithm-dependent role in mapping fuel consumption. Whereas the direct consumption mapping approach (KDC) benefitted greatly from the inclusion of Landsat change metrics in modeling fuel consumption, the indirect approach (MFLC) saw no tangible improvements. One possible reason Landsat was so helpful to KDC may be its temporal consistency. The two airborne lidar datasets compared in this study were collected using different sensors, on different aircraft, flying different patterns, yielding different point cloud densities. Thus, the direct comparison of point cloud data naturally yields some degree of noise, giving the appearance of vegetation structural change in some places where no such change took place in reality. This is evident in the lidar-only mapped results, especially for KDC models, where sometimes relatively high consumption totals were predicted outside of areas known to have burned. However, Landsat, being a highly calibrated, spaceborne sensor with spatiotemporally consistent, repeat measurements enabled a clearer distinction between burned and unburned areas, refining the lidar-based predictions in the KDC models. Therefore, it served to more clearly distinguish signal (i.e., fire-induced fuel load changes) from noise (i.e., changes in mapped point cloud structure not caused by fire). Furthermore, the lidar data only provided two snapshots in time in a dynamic landscape that has featured several non-fire disturbances (e.g., mechanical thinning, insect mortality, etc.) at various times between those snapshots. Given that annual Landsat data were used, with metrics designed to capture year-to-year change, Landsat would have been able to make clearer distinctions between change and non-change. It is possible that including a greater proportion of "control" plots, where no disturbances took place, into the KDC training data would have improved their lidar-only predictions of burned versus unburned areas. There are a variety of other approaches to quantifying spectral change over time that we could have employed, including well-established time series algorithms such as Landtrendr (Kennedy et al., 2010) and Continuous Change Detection and Classification (CCDC) (Zhu and Woodcock, 2014). Although our comparably simple and parameter-free time series metrics proved valuable to predicting fuel consumption, future research may aim to investigate the predictive value added from the use of more advanced time series algorithms.

A noteworthy limitation of this study is the time differences between fuel plot sampling and lidar scanning. The pre-fire and post-fire lidar data were flown in 2016 and 2023, respectively. The pre-fire fuels data were measured between 2016 and 2019. The difference between pre-fire fuel conditions when scanned and measured likely posed little challenge to the success of our predictive models, given the fact that mature forests undisturbed by fire for decades are unlikely to experience substantial fuel load changes over the course of three years. However, post-fire fuels

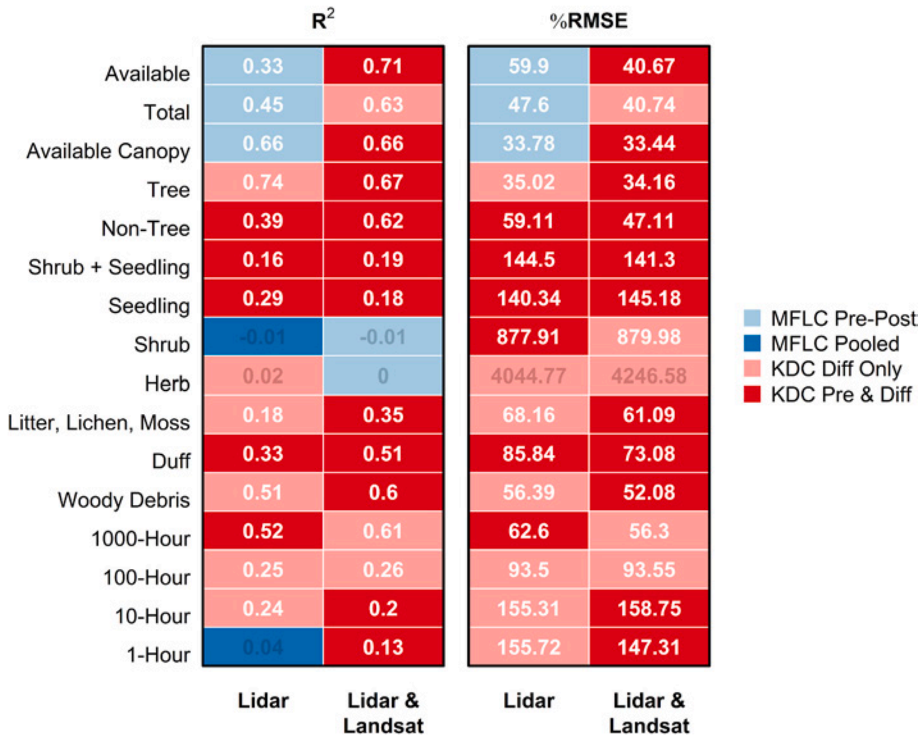

Fig. 8. The best-performing model type for each fuelbed (row) and associated performance metrics, according to R^2 (left) and %RMSE (right). In each case, the left column represents the model with just lidar-based predictor variables and the right column represents the model with both lidar- and Landsat-based predictor variables. Performance metrics for models with significant ($p < 0.01$) non-zero slopes between predictions and observations are shown with white text.

were measured between 2019 and 2021 – in some cases as long as four years before the post-fire lidar data were collected. Post-fire revegetation can drive significant fuel development on relatively short time scales, as canopy clearing can promote rapid growth of understory vegetation. Furthermore, felling of fire-killed snags can promote the rapid accumulation of surface fuels. Some combination of these phenomena are evident in Figs. 4 and 9, which show accumulation in the 1–2.5 m height range post-fire. Although post-fire lidar data were collected in 2020 and 2021, their spatial extents were limited to a buffered area around a selection of fire perimeters, which inhibited the ability to map consumption across the entire study area (McCarley et al., 2024). Given Monroe Mountain's rich, recent history of fire activity, we opted to use a more recent but much larger dataset to facilitate a broader-scale analysis of fuel consumption.

At its core, KDC – the best-performing model type tested in our study – is based on the conversion of a discrete return point cloud into a continuous, waveform-like energetic distribution based on vertical point densities. It is worth noting that no return intensity information was used in the generation of kernel density profiles, which would be important for a more accurate point cloud to waveform approximation (Hancock et al., 2019). Nevertheless, KDC's wave-like nature brings about an important question regarding the degree to which waveform lidar instruments could potentially be used for direct fuel consumption estimation. GEDI, for one important example, could potentially be used in conjunction with airborne lidar data in a KDC modeling context to map fuel consumption, and potentially other forest biomass losses, on broad spatial scales (Dubayah et al., 2020). GEDI data have been applied to quantifying fire-induced vegetation structural changes in several recent studies (e.g., Guerra-Hernández et al., 2024; Huettermann et al., 2023; Pascual and Guerra-Hernández, 2023). Future research should aim to apply a KDC analysis framework to mapping fuel consumption using real or simulated GEDI data.

One of KDC's strengths is its relative simplicity. It only requires two parameters: (1) the kernel's bandwidth (we selected 5 cm); and (2) the heights at which kernel density is to be estimated (we selected 0–20 m at a 10 cm interval). Although an extensive evaluation of the sensitivity of these parameters on fuel consumption predictive ability was beyond the scope of this study, future KDC users should carefully consider them in the context of their own fuel type and fire regime. For example, in shorter fuels (i.e., shrublands or grasslands), a smaller bandwidth at a narrower but more densely sampled range of heights may be useful for capturing finer-scale consumption. The bandwidth and height interval should be considered together; a smaller bandwidth should generally be used in conjunction with a smaller height interval to ensure that the full vertical fuel profile is captured among the set of KDC predictor variables. However, too small of a bandwidth and height interval will yield an excessive number of predictors that could be subject to overfitting. Conversely, too large of a bandwidth and height interval could fail to capture the structural nuance of fuel consumption in different fuelbeds. Even with the same bandwidth and height interval, KDC calculated at different heights (e.g., 1 cm, 11 cm, and 21 cm instead of 0 cm, 10 cm, and 20 cm) would yield slightly different values. One potential approach for minimizing these height-specific effects would be to integrate kernel densities over a range of heights. However, this would require careful definition of the defined height ranges of interest to avoid obscuring fine-scale fuel consumption.

Across model types, fuel consumption predictive performance varied substantially by fuelbed. Poor performance in some fuelbeds may be attributable to some combination of three factors: (1) a poor distribution of consumption values being fed to the models; (2) the inability of the remote sensing data to distinguish between narrowly defined fuelbeds; and (3) uncertainty in the field data. With respect to the first factor, Figures A2-A9 show that the distribution of herb and shrub consumption values, both of which performed very poorly, are ill-suited for training a machine learning model, given their lack of observed variability. Regarding the second factor, at least with airborne or satellite data, there is little hope that a remotely sensed dataset can distinguish between, for example, similarly sized 1-h fuels and 10-h fuel loads. The only hope for accurate modeling of consumption in these narrowly defined fuelbeds is that their consumption is uniquely correlated with

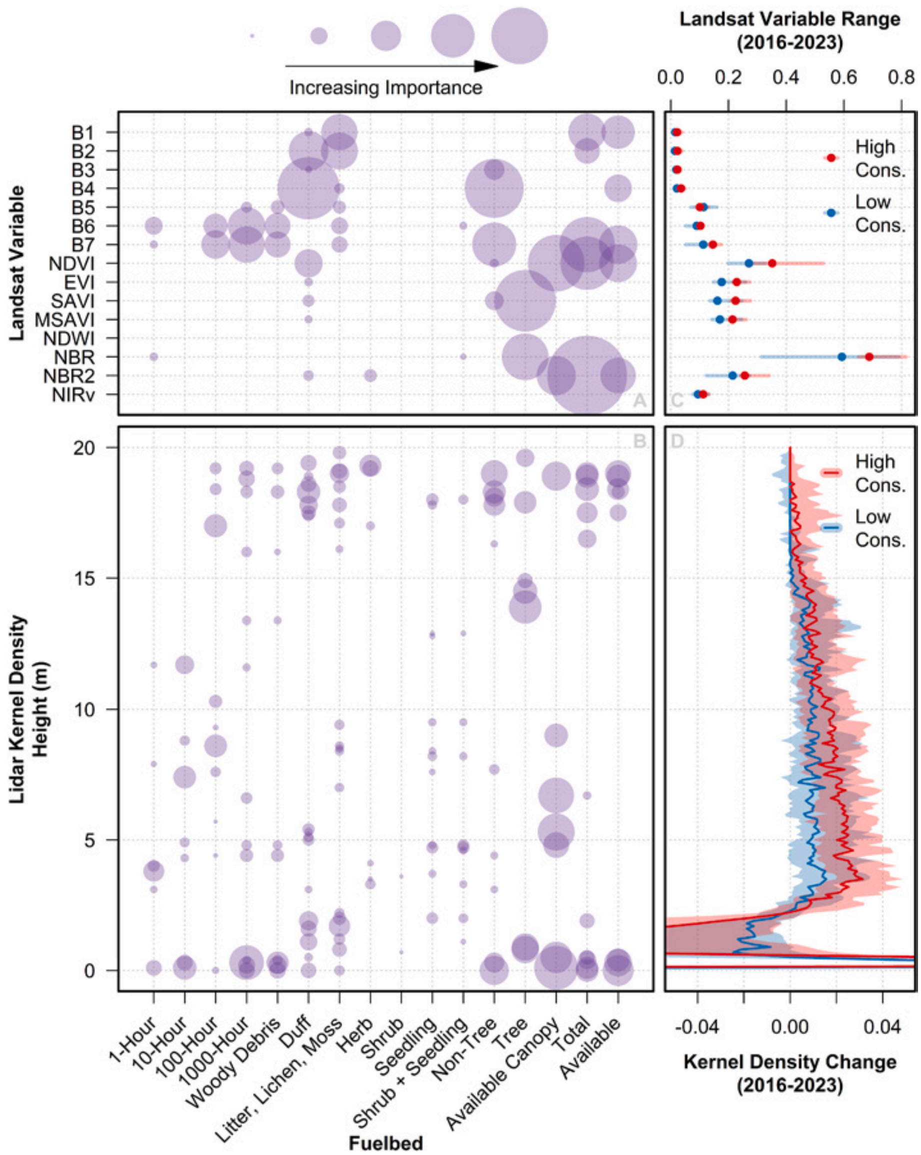

Fig. 9. A summary of variable importance across the four KDC-based models (KDC Diff Only: Lidar; KDC Diff Only: Lidar + Landsat; KDC Pre & Diff: Lidar; and KDC Pre & Diff: Lidar + Landsat). Points in (A) and (B) represent the selection of a predictor variable by VSURF in at least one of the four models, sized according to their mean importance among the four models, as measured by the percent increase in mean squared error that would result by randomly permuting predictor variable values. Note that Landsat predictors were only included in two of the four models, so (A) represents mean importance among two models and (B) represents mean importance among four models. (C) and (D) highlight predictor-response relationships by comparing relatively high consumption plots to relatively low consumption plots. (C) represents the range (maximum absolute difference) in the Landsat time series, with the points representing the median range values and the lines representing the interquartile ranges among "high" and "low" consumption plots. (D) represents the medians (solid lines) and interquartile ranges (semitransparent polygons) among "high" and "low" consumption plots.

other structural changes that can be better approximated by remotely sensed data. This is evident in the KDC variable importance analysis (Fig. 9), where variables near the canopy top were selected as predictors of surface and ground fuels. In this sense, canopy KDC metrics were not serving as direct measures of change in surface/ground fuel consumption, but usefully correlated proxies thereof. We do not propose KDC as a physically-based model, whereby change in lidar point kernel density at a height strictly corresponds to, and is the sole basis of estimating, fuel consumption at that height. Instead, KDC yields a suite of change metrics across a range of heights whose combinations may be statistically related to consumption in particular fuelbeds. Although lidar has impressive vegetation structural mapping capability, laser pulse absorption in the canopy can inhibit accurate representation of the understory (Campbell et al., 2018). Accordingly, low lidar point kernel density in a lower height stratum could occur in an area that features low surface fuel loads or one that features high surface fuel loads and simply has a dense, absorptive canopy. Lastly, the field data themselves, and how they correspond spatially with the remotely sensed data, may have driven some degree of uncertainty. For example, tree and canopy fuel consumption yielded some of the best model performance. These fuels were also measured over the largest area – either an 8 m or 5.6 m radius circle (Fig. 2) – which aligns better spatially with the 8 m radius circular area that was used to clip lidar and Landsat data. On the opposite extreme, fine woody debris, herbs, shrubs, and seedlings were collected in comparably very small 0.25 m^2 or 1 m^2 subplots, with differing locations pre- and post-fire. Thus, we were left to assume that consumption in these small areas would be representative of consumption within the entire 8 m-radius analysis area.

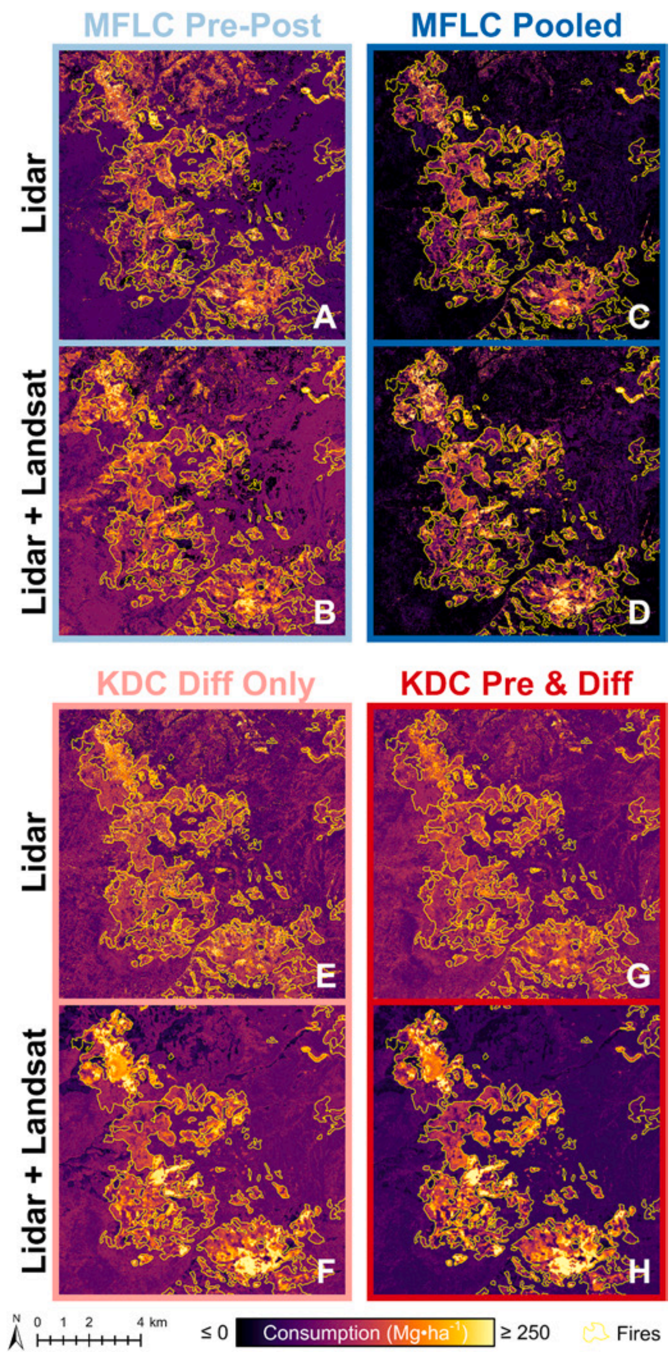

Fig. 10. Fuel consumption maps for total fuels predicted by each of the eight model types tested in this study. Maps focus on an area within Monroe Mountain that featured several prescribed fires between 2016 and 2023. The fire perimeters are approximated and derived from thresholding of Landsat normalized burn ratio differences between successive years within the time frame (2016–2023).

5. Conclusions

Precise, spatially explicit quantification of fuel consumed in wildland fires has many downstream scientific benefits, ranging from improved understanding of the carbon cycle to more accurate estimation of emissions. In this study, we introduced KDC, a new and improved approach to directly mapping consumption in a diverse array of fuelbeds using multitemporal lidar. Although performance by fuelbed varied, with more aggregated fuelbeds and those related to tree fuels yielding better results, KDC was still able to predict some of the more challenging ground and surface fuelbeds better than the more common, indirect approach provided by MFLC. Although MFLC was generally outperformed, it does possess some unique benefits not provided by KDC, including the fact that it does not rely on bitemporal, spatially coincident field measurements of fuel loads. Such opportunities present themselves with prescribed fires (as in this study) but would be rare with wildfires. The inclusion of Landsat spectral change metrics greatly benefitted KDC's ability to model consumption; therefore, we suggest that future efforts to employ KDC consider the use of Landsat or other time series image data to improve predictive ability. Future research should aim to test the robustness of KDC in other landscapes where multitemporal lidar and fuel measurements are available. Future research should also explore whether KDC could be generalized using field measurements from a variety of different fuel and fire contexts, and whether KDC could be applied to lidar data collected from other platforms, such as terrestrial, mobile, or spaceborne lidar.

Lastly, although the focus of this study was on fuel consumption due to wildland fire, KDC should be responsive to structural changes driven by other disturbance agents as well. This research demonstrated that finer-particle fuelbeds with smaller load changes were generally more difficult to predict. Accordingly, KDC and other bitemporal lidar change approaches may struggle to capture subtle structural changes (e.g., diffuse insect defoliation). However, KDC may excel in quantifying more stark biomass losses due to windthrow or harvesting. Future research should focus on KDC's ability to accurately predict biomass change driven by a wider range of disturbance agents.

CRediT authorship contribution statement

Michael J. Campbell: Writing – review & editing, Writing – original draft, Visualization, Validation, Supervision, Software, Project administration, Methodology, Investigation, Funding acquisition, Formal analysis, Data curation, Conceptualization. **Andrew T. Hudak:** Writing – review & editing, Supervision, Resources, Project administration, Methodology, Funding acquisition, Conceptualization. **T. Ryan McCarley:** Writing – review & editing, Validation, Data curation. **Benjamin C. Bright:** Writing – review & editing, Validation, Data curation. **Philip E. Dennison:** Writing – review & editing, Supervision, Resources, Project administration, Methodology, Funding acquisition, Conceptualization.

Funding

This work was supported by the USDA Forest Service (USFS) Fire And Smoke Model Evaluation Experiment (FASMEE) through a Challenge Cost Share Agreement between the USFS Rocky Mountain Research Station and the University of Utah (22-CS-11221633-163). This work was also supported by a NASA FireSense Implementation Team grant (80NSSC24K1310). This research was supported (in part) by the U.S. Department of Agriculture, Forest Service. Any use of trade, firm, or product names is for descriptive purposes only and does not imply endorsement by the U.S. government.

Declaration of competing interest

The authors declare the following financial interests/personal relationships which may be considered as potential competing interests: Michael Campbell reports financial support was provided by US Department of Agriculture Forest Service. Michael Campbell reports financial support was provided by NASA. If there are other authors, they declare that they have no known competing financial interests or personal relationships that could have appeared to influence the work reported in this paper.

Appendix A. Additional Figures

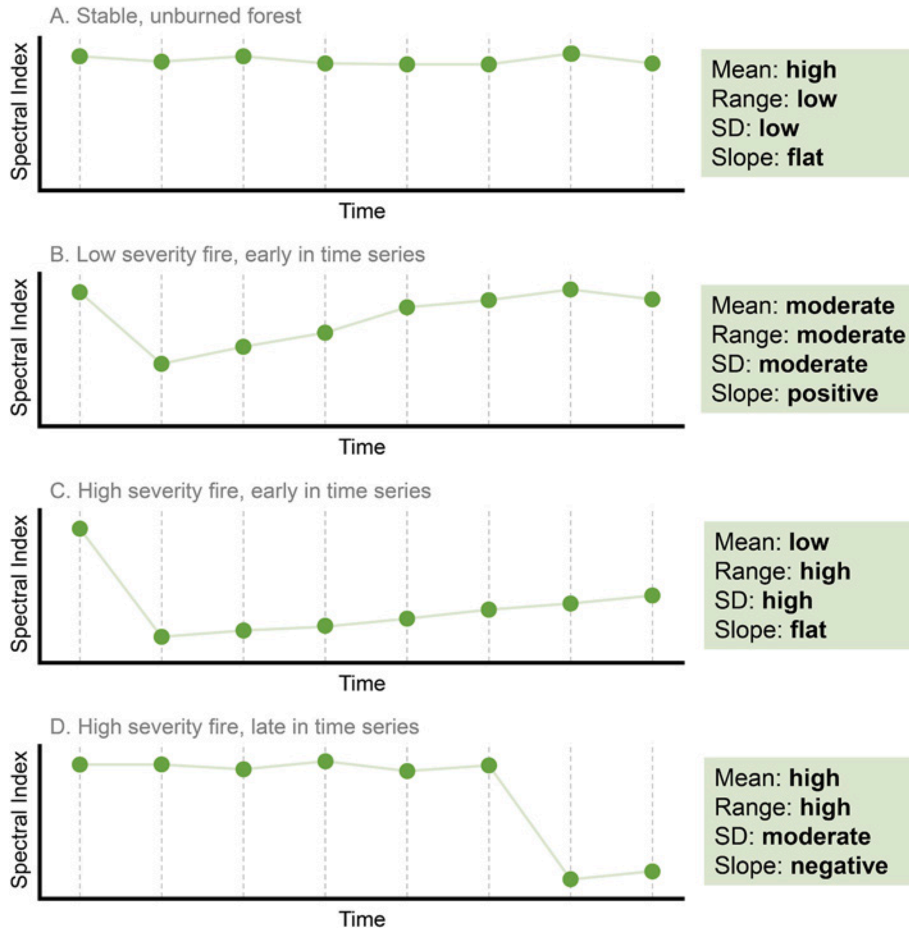

Fig. A1. Theoretical Landsat spectral index time series representing four different scenarios that capture a range of fire presence/absence, severity, and timing, highlighting the novel contribution of each of the four time series metrics: mean, range, standard deviation (SD), and regression slope.

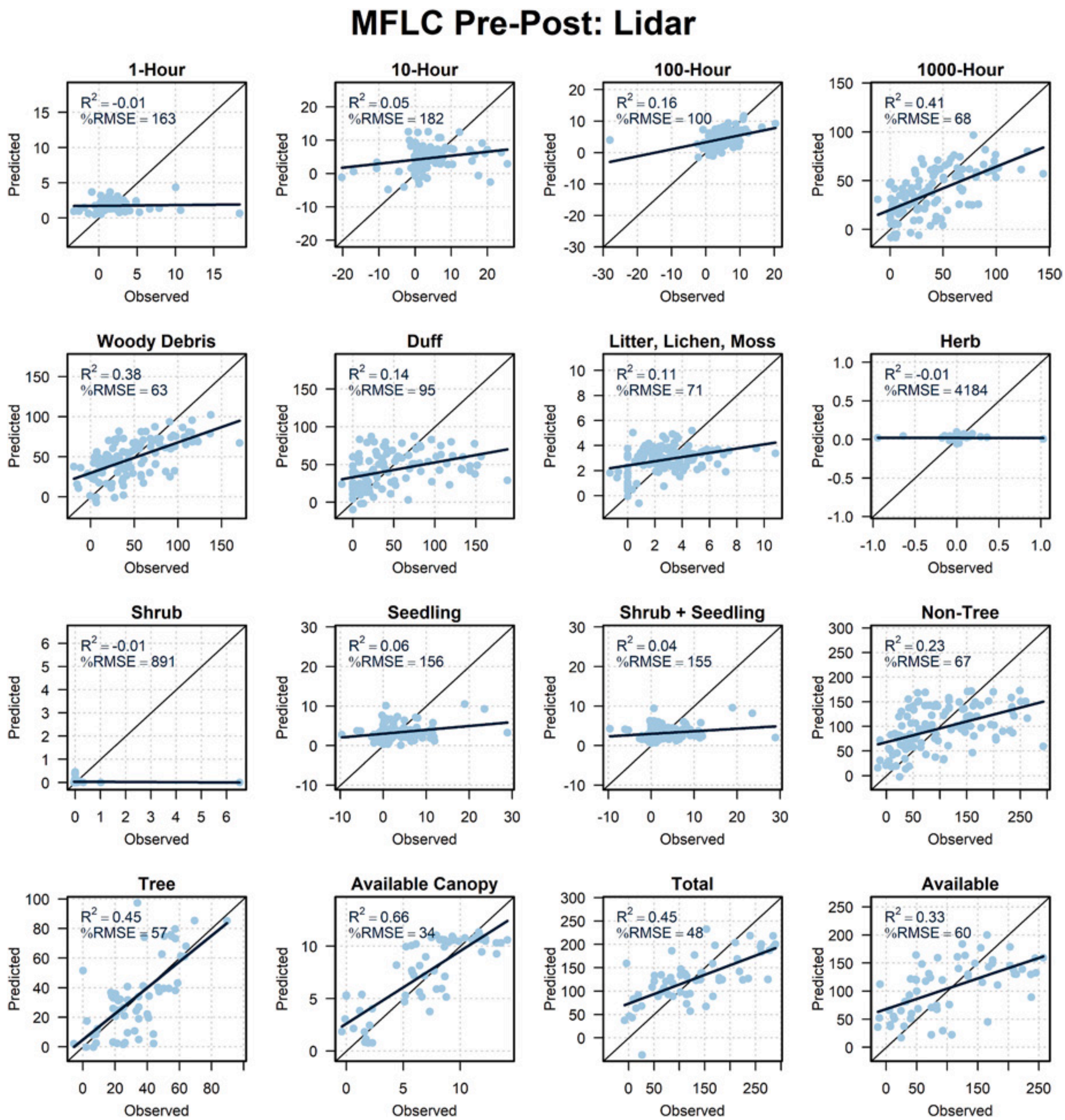

Fig. A2. Predictions versus observations for all modeled fuelbeds using the MFLC Pre-Post model with just lidar predictors.

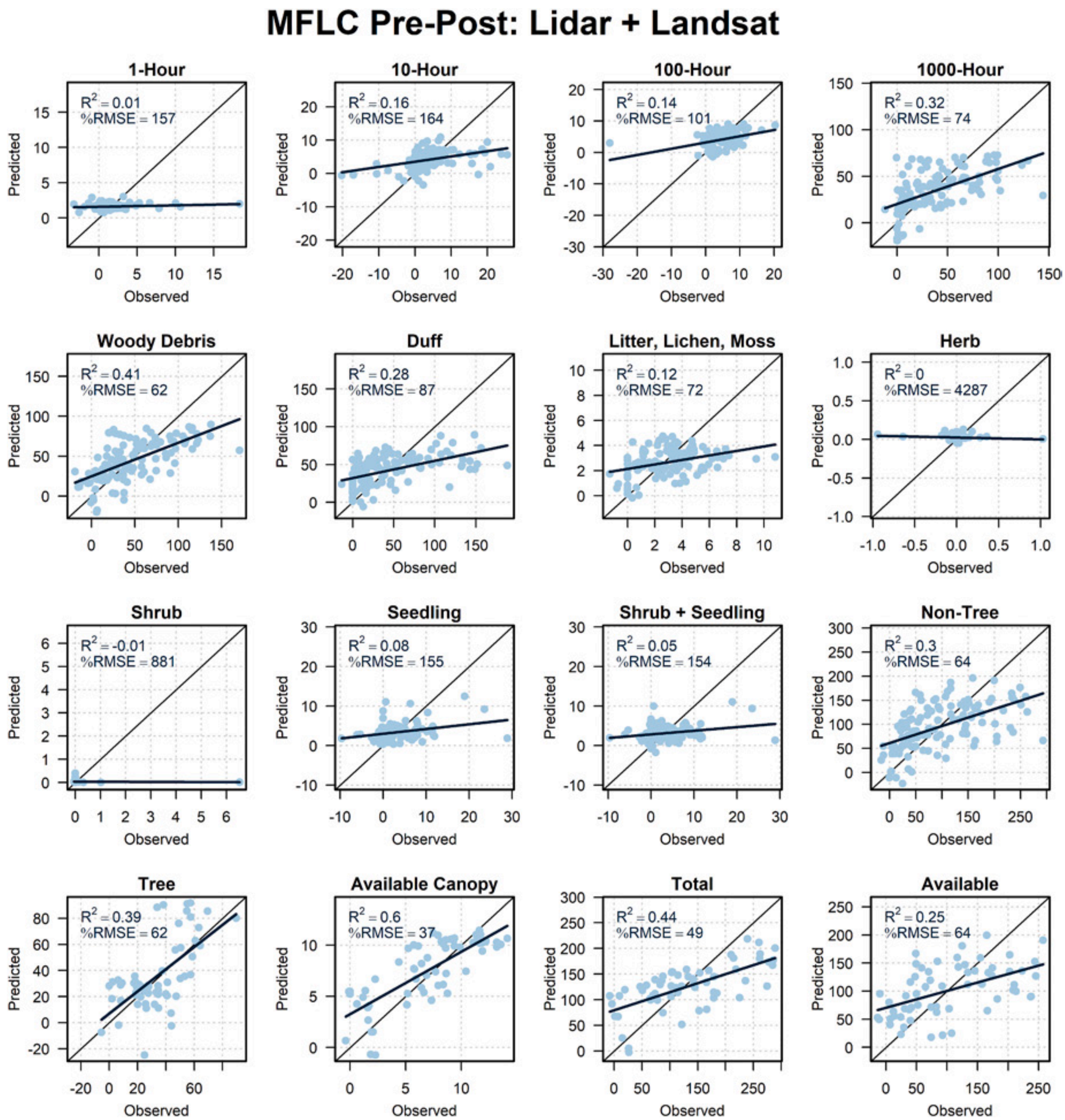

Fig. A3. Predictions versus observations for all modeled fuelbeds using the MFLC Pre-Post model with lidar and Landsat predictors.

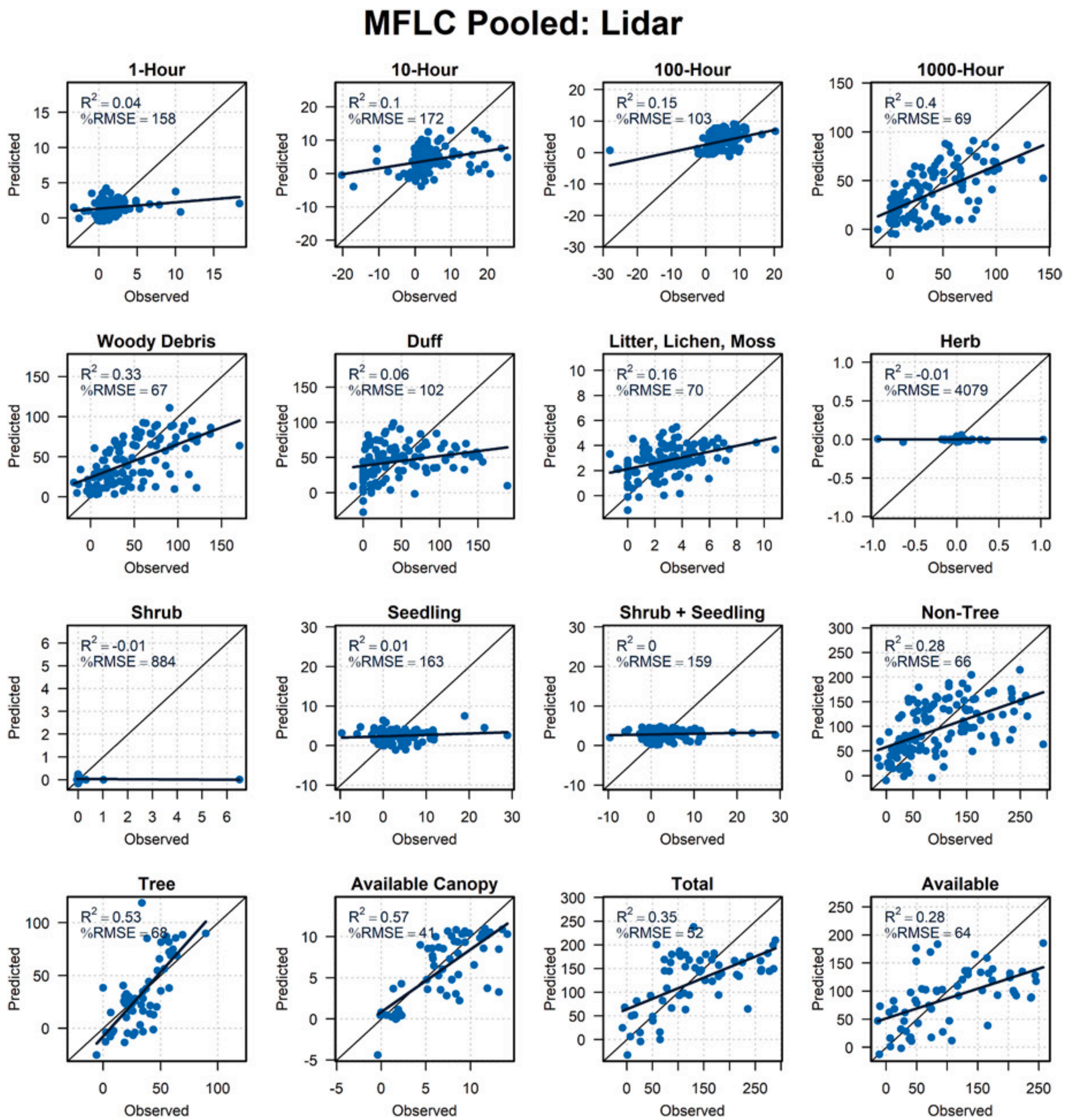

Fig. A4. Predictions versus observations for all modeled fuelbeds using the MFLC Pooled model with just lidar predictors.

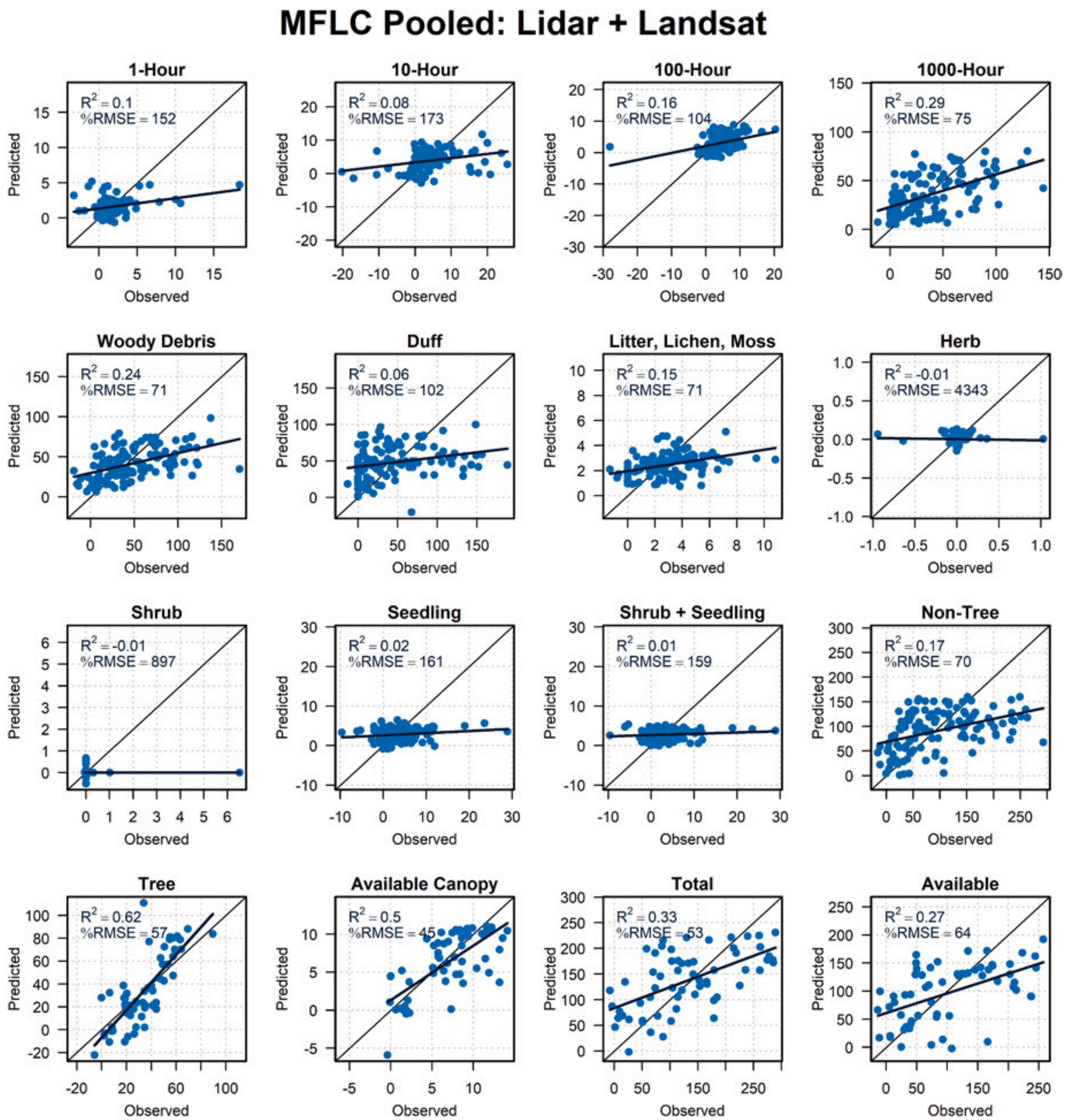

Fig. A5. Predictions versus observations for all modeled fuelbeds using the MFLC Pre-Post model with lidar and Landsat predictors.

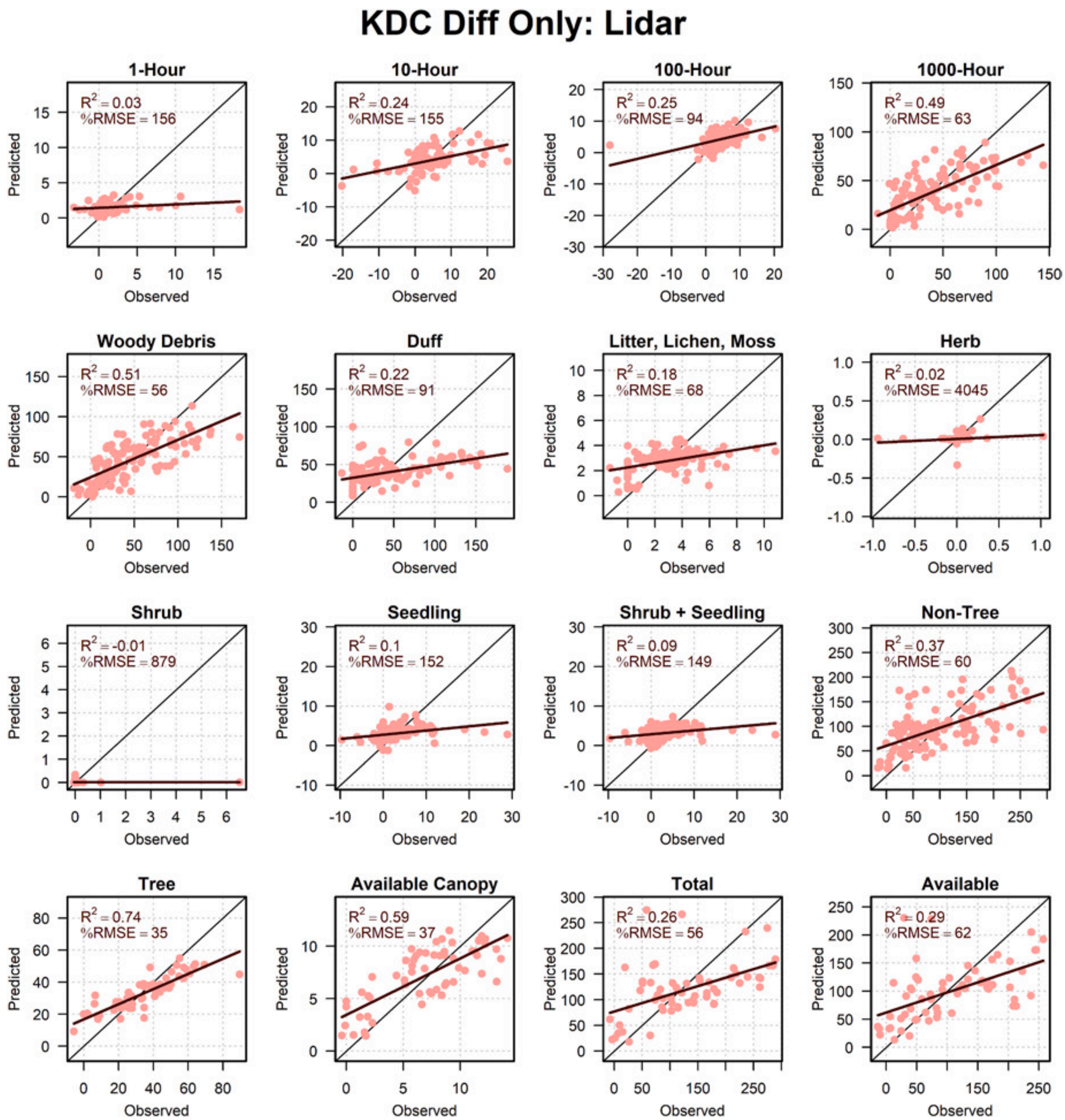

Fig. A6. Predictions versus observations for all modeled fuelbeds using the KDC Diff Only model with just lidar predictors.

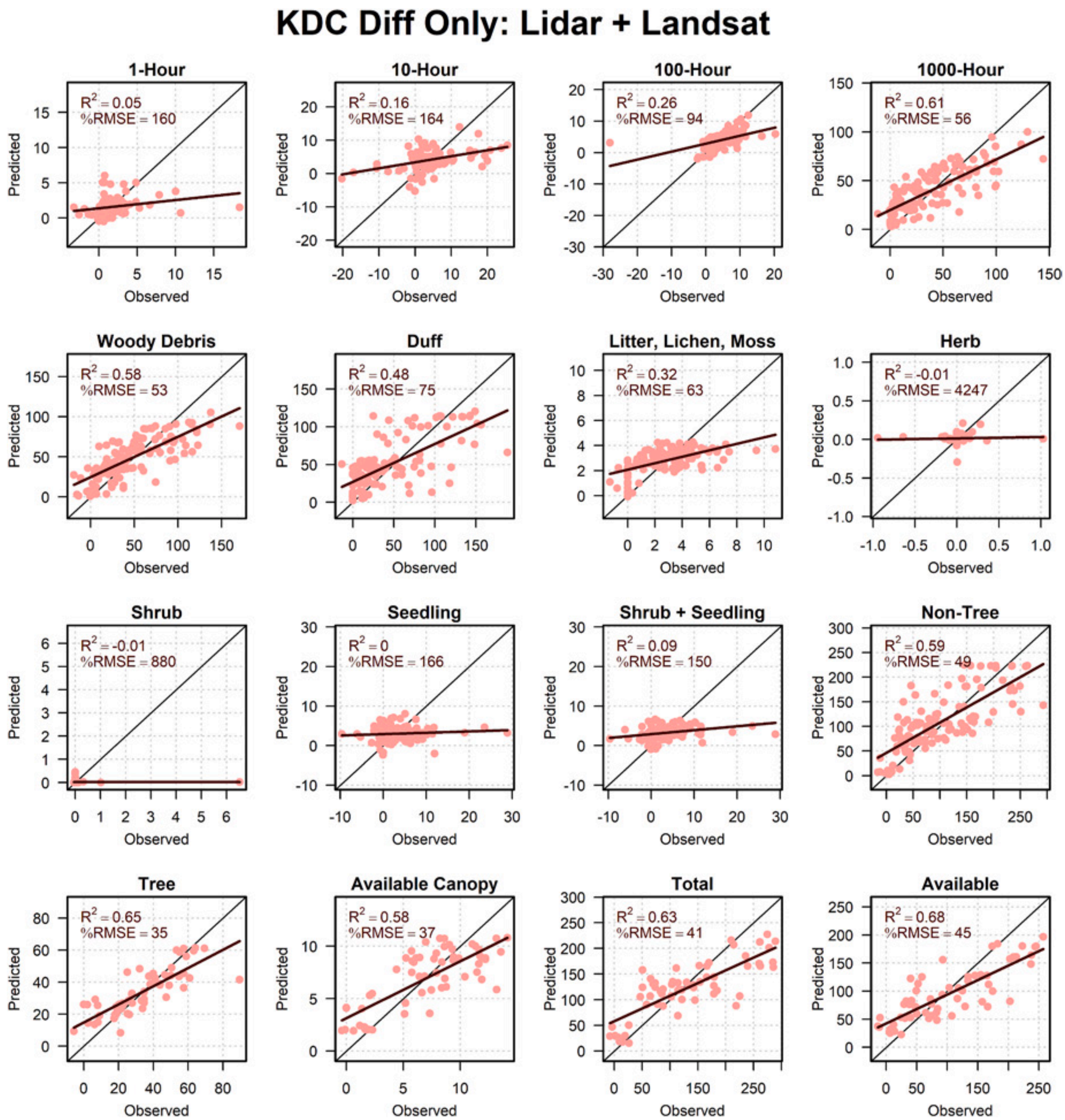

Fig. A7. Predictions versus observations for all modeled fuelbeds using the KDC Diff Only model with lidar and Landsat predictors.

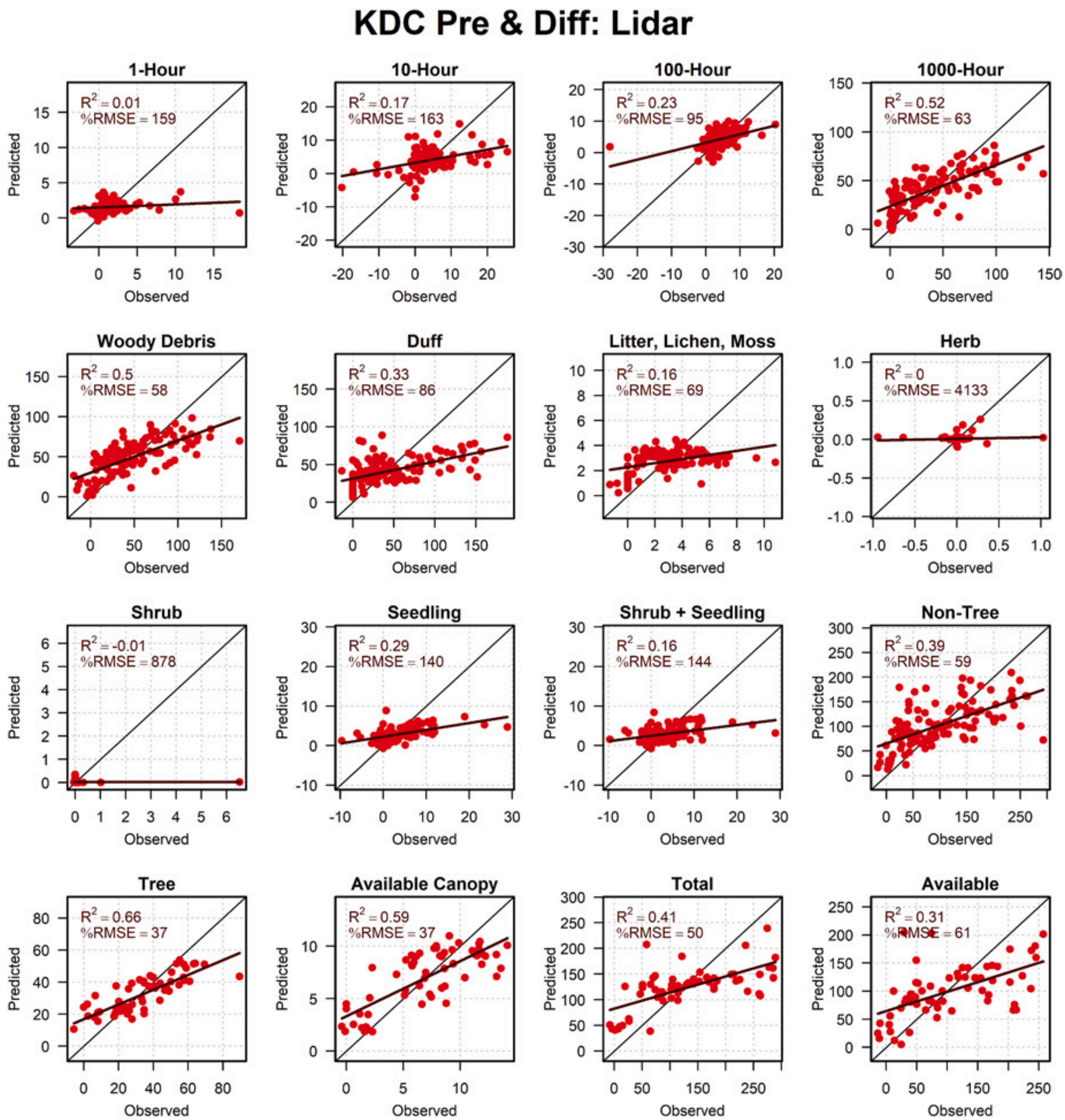

Fig. A8. Predictions versus observations for all modeled fuelbeds using the KDC Pre & Diff model with just lidar predictors.

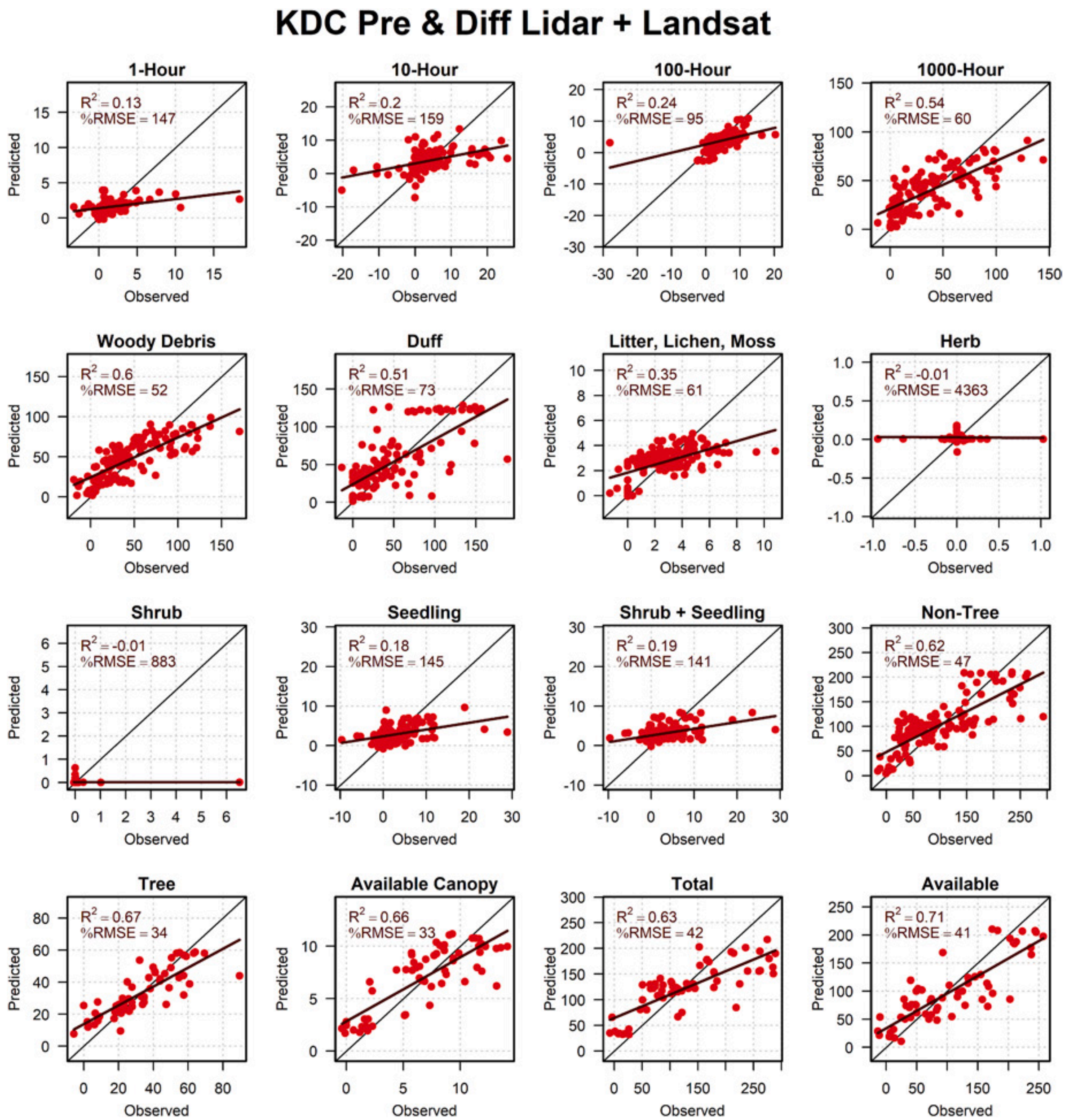

Fig. A9. Predictions versus observations for all modeled fuelbeds using the KDC Pre & Diff model with lidar and Landsat predictors.

Appendix B. Evaluating the Potential of Combining MFLC and KDC

Although the core focus of this study is a comparative analysis between fuel consumption mapping approaches, the overarching objective of this work is to improve our ability to estimate fuel consumption using remotely sensed data. Given that the two approaches compared in this study (MFLC and KDC) rely on the same input datasets (pre- and post-fire airborne lidar data, Landsat data, and fuels data), it is conceivable that a hybrid approach could be developed that incorporates elements of both in a singular predictive model. For example, perhaps pre- and post-fire kernel densities would add useful predictive ability to the indirect MFLC models. Alternatively, perhaps incorporating changes in the MFLC predictor variables (i.e., lidar metrics derived from the *lidRmetrics* library (Tompalski, 2023)) between the two time frames would improve direct KDC predictive accuracy. We explored both of these options, as follows:

1. **Direct approach (KDC-centric):** There were four KDC models tested in this study: (1) KDC Diff Only: Lidar; (2) KDC Diff Only: Lidar + Landsat; (3) KDC Pre & Diff: Lidar; and (4) KDC Pre & Diff: Lidar + Landsat. For each of these four models, we compared their original fuel consumption predictive performance (R^2 and %RMSE) to that when differences between pre- and post-fire structural metrics from *lidRmetrics* (Tompalski, 2023) were added to the suite of candidate predictor variables. There were 85 change metrics added to those enumerated in Table 2. This analysis investigated the degree to which additional lidar structural change metrics beyond the relatively simple KDC metrics would enhance predictive ability.

2. **Indirect approach (MFLC-centric):** There were four MFLC models tested in this study: (1) MFLC Pre-Post: Lidar; (2) MFLC Pre-Post Lidar + Landsat; (3) MFLC Pooled: Lidar; and (4) MFLC Pooled: Lidar + Landsat. For each of these four models, we compared their original fuel consumption predictive performance (R^2 and %RMSE) to that when pre- and post-fire kernel densities were added to the suite of candidate predictor variables. There were 201 pre-fire kernel densities (0–20m at 0.1m interval) and 201 post-fire kernel densities, adding 402 candidate predictor variables to those enumerated in Table 2. The fundamental question this analysis sought to answer surrounded the potential explanatory power of kernel densities above and beyond those contained within the diverse array of original lidar structural predictor variables.

In all, eight new types of models were evaluated for each of the 16 fuelbeds (Table A1; Figures A10-A11). Overall, the performance of the combined models did not yield consistent improvements over the original models. Although R^2 values generally improved slightly, the difference between original and combined model R^2 values was only significant for three out of the eight models based on a paired *t*-test. %RMSE actually increased in more instances than it decreased, but none of the changes were found to be statistically significant. Accordingly, while correlations between predicted and observed fuel consumption tended to improve incrementally, the predictive error rarely improved and often worsened. Especially when considering the added complexity of combining these predictor variables, these results point towards the fact that combined approaches do not yield worthwhile performance gains over the original models.

Table A1
Mean difference in model performance (R^2 and %RMSE) among the 16 fuelbeds evaluated in this study between the original KDC/MFLC models and the combined models.

Model Type	Mean R^2 Difference	Mean %RMSE Difference
Direct Diff Only: Lidar	+0.006	+6.260
Direct Diff Only: Lidar + Landsat	+0.022*	−4.539
Direct Pre & Diff: Lidar	−0.001	+1.223
Direct Pre & Diff: Lidar + Landsat	+0.011	−16.242
Indirect Pre-Post: Lidar	+0.048*	+4.725
Indirect Pre-Post: Lidar + Landsat	+0.027	+20.902
Indirect Pooled: Lidar	+0.045*	+5.560
Indirect Pooled: Lidar + Landsat	+0.029	+3.488

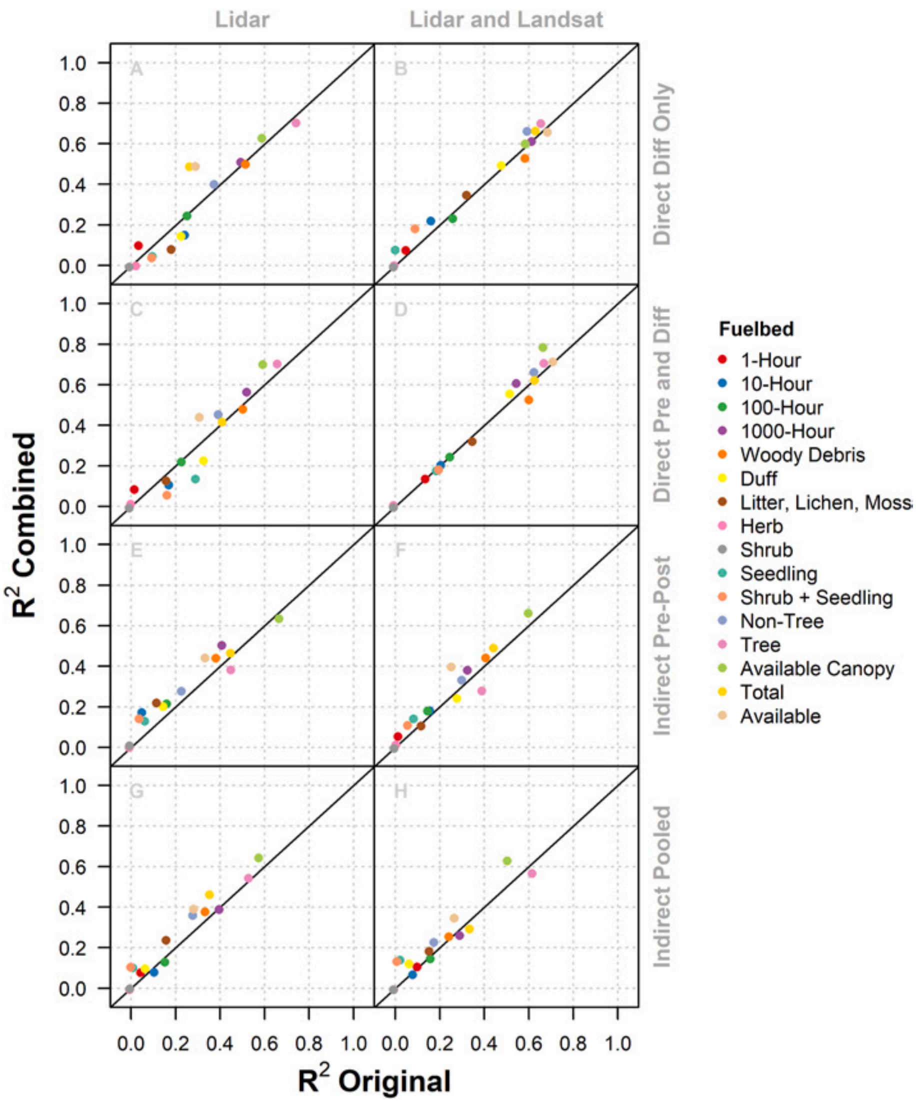

Fig. A10. Difference in R^2 among the 16 fuelbeds evaluated in this study between the original KDC/MFLC models and the combined models.

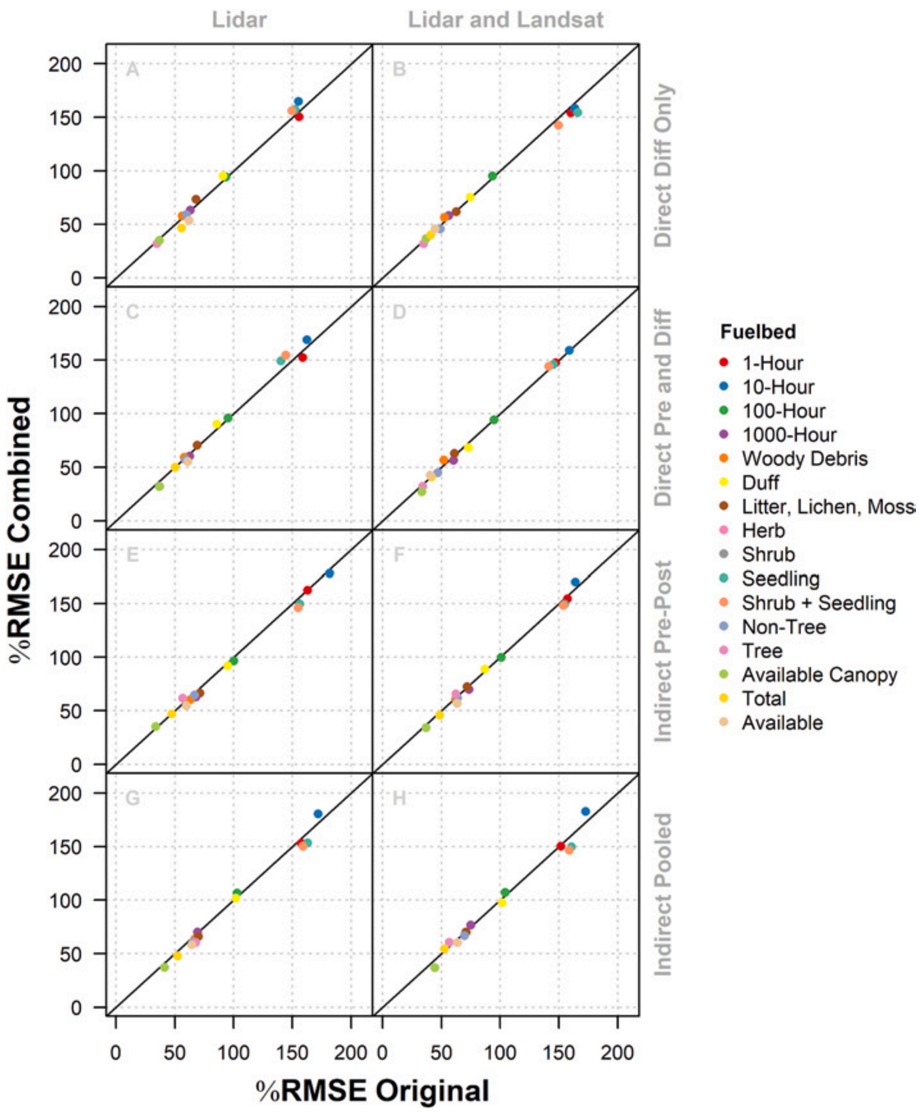

Fig. A11. Difference in %RMSE among the 16 fuelbeds evaluated in this study between the original KDC/MFLC models and the combined models. Note that these plots are focused on the %RMSE ranges that encompassed most of the well-performing models, and do not show outliers with extreme %RMSE values.

Data availability

Data will be made available on request.

References

Bergstra, J., Bengio, Y., 2012. Random search for hyper-parameter optimization. J. Mach. Learn. Res. 13.

Bollandsås, O.M., Gregoire, T.G., Næsset, E., Øyen, B.-H., 2013. Detection of biomass change in a Norwegian Mountain forest area using small footprint airborne laser scanner data. Stat. Methods Appl. 22, 113–129. https://doi.org/10.1007/s10260-012-0220-5.

Breiman, L., 2001. Random forests. Mach. Learn. 45, 5–32. https://doi.org/10.1023/A:1010933404324.

Bright, B.C., Hudak, A.T., Kennedy, R.E., Braaten, J.D., Henareh Khalyani, A., 2019. Examining post-fire vegetation recovery with landsat time series analysis in three Western North American forest types. fire ecol 15, 8. https://doi.org/10.1186/s42408-018-0021-9.

Bright, B.C., Hudak, A.T., McCarley, T.R., Spannuth, A., Sánchez-López, N., Ottmar, R.D., Soja, A.J., 2022. Multitemporal lidar captures heterogeneity in fuel loads and consumption on the kaibab Plateau. fire ecol 18, 18. https://doi.org/10.1186/s42408-022-00142-7.

Brodrick, P.G., Asner, G.P., 2017. Remotely sensed predictors of conifer tree mortality during severe drought. Environ. Res. Lett. 12, 115013. https://doi.org/10.1088/1748-9326/aa8f55.

Brown, J.K., Oberheu, R.D., Johnston, C.M., 1982. Handbook for inventorying surface fuels and biomass in the interior west. Gen. Tech. Rep. INT-GTR-129. Ogden, UT: U. S. Department of Agriculture, Forest Service, Intermountain Forest and Range Experimental Station 48, 129. https://doi.org/10.2737/INT-GTR-129.

Butler, B.W., 2014. Wildland firefighter safety zones: a review of past science and summary of future needs. Int. J. Wildland Fire 23, 295–308. https://doi.org/10.1071/WF13021.

Campbell, M.J., Dennison, P.E., Hudak, A.T., Parham, L.M., Butler, B.W., 2018. Quantifying understory vegetation density using small-footprint airborne lidar. Rem. Sens. Environ. 215, 330–342. https://doi.org/10.1016/j.rse.2018.06.023.

Campbell, M.J., Dennison, P.E., Tune, J.W., Kannenberg, S.A., Kerr, K.L., Codding, B.F., Anderegg, W.R.L., 2020. A multi-sensor, multi-scale approach to mapping tree mortality in woodland ecosystems. Rem. Sens. Environ. 245, 111853. https://doi.org/10.1016/j.rse.2020.111853.

Campbell, M.J., Williams, J.P., Berryman, E.M., Anderegg, W.R.L., 2024. Quantifying current and potential future impacts of balsam woolly adelgid infestation on forest biomass. For. Ecol. Manag. 560, 121852. https://doi.org/10.1016/j.foreco.2024.121852.

Cao, L., Coops, N.C., Innes, J.L., Sheppard, S.R.J., Fu, L., Ruan, H., She, G., 2016. Estimation of forest biomass dynamics in subtropical forests using multi-temporal airborne LiDAR data. Rem. Sens. Environ. 178, 158–171. https://doi.org/10.1016/j.rse.2016.03.012.

Clark, K.L., Heilman, W.E., Skowronski, N.S., Gallagher, M.R., Mueller, E., Hadden, R.M., Simeoni, A., 2020. Fire behavior, fuel consumption, and turbulence and energy exchange during prescribed fires in pitch pine forests. Atmosphere 11, 242. https://doi.org/10.3390/atmos11030242.

Crawford, C.J., Roy, D.P., Arab, S., Barnes, C., Vermote, E., Hulley, G., Gerace, A., Choate, M., Engebretson, C., Micijevic, E., Schmidt, G., Anderson, C., Anderson, M., Bouchard, M., Cook, B., Dittmeier, R., Howard, D., Jenkerson, C., Kim, M., Kleyians, T., Maiersperger, T., Mueller, C., Neigh, C., Owen, L., Page, B., Pahlevan, N., Rengarajan, R., Roger, J.-C., Sayler, K., Scaramuzza, P., Skakun, S., Yan, L., Zhang, H.K., Zhu, Z., Zahn, S., 2023. The 50-year landsat collection 2 archive. Science of Remote Sensing 8, 100103. https://doi.org/10.1016/j.srs.2023.100103.

Dalponte, M., Jucker, T., Liu, S., Frizzera, L., Gianelle, D., 2019. Characterizing forest carbon dynamics using multi-temporal lidar data. Rem. Sens. Environ. 224, 412–420. https://doi.org/10.1016/j.rse.2019.02.018.

Daly, C., Taylor, G.H., Gibson, W.P., 1997. The PRISM approach to mapping precipitation and temperature. In: Proc., 10th AMS Conf. on Applied Climatology, pp. 20–23.

Dubayah, R., Blair, J.B., Goetz, S., Fatoyinbo, L., Hansen, M., Healey, S., Hofton, M., Hurtt, G., Kellner, J., Luthcke, S., Armston, J., Tang, H., Duncanson, L., Hancock, S., Jantz, P., Marselis, S., Patterson, P.L., Qi, W., Silva, C., 2020. The global ecosystem dynamics investigation: high-Resolution laser ranging of the Earth's forests and topography. Science of Remote Sensing 1, 100002. https://doi.org/10.1016/j.srs.2020.100002.

Eagle, P.C., Cronan, J.B., McCarley, T.R., Bright, B.C., Hudak, A.T., 2024. Field plot measurements from the 2017-2020 FASMEE Rx fires. https://doi.org/10.2737/RDS-2024-0049.

Eidenshink, J., Schwind, B., Brewer, K., Zhu, Z.L., Quayle, B., Howard, S., 2007. Project for monitoring trends in burn severity. Fire Ecol. 3 (1), 3–21.

Einzmann, K., Immitzer, M., Böck, S., Bauer, O., Schmitt, A., Atzberger, C., 2017. Windthrow detection in European forests with very high-resolution optical data. Forests 8, 21. https://doi.org/10.3390/f8010021.

Engelstad, P.S., Falkowski, M., Wolter, P., Poznanovic, A., Johnson, P., 2019. Estimating canopy fuel attributes from low-density LiDAR. Fire 2, 38. https://doi.org/10.3390/fire2030038.

Finney, M.A., 2001. Design of regular landscape fuel treatment patterns for modifying fire growth and behavior. For. Sci. 47, 219–228. https://doi.org/10.1093/forestscience/47.2.219.

Fisher, G.B., Elmore, A.J., Fitzpatrick, M.C., McNeil, D.J., Atkins, J.W., Larkin, J.L., 2024. Mapping recent timber harvest activity in a temperate forest using single date airborne LiDAR surveys and machine learning: lessons for conservation planning. GIScience Remote Sens. 61, 2379198. https://doi.org/10.1080/15481603.2024.2379198.

French, N.H.F., Goovaerts, P., Kasischke, E.S., 2004. Uncertainty in estimating carbon emissions from boreal forest fires. J. Geophys. Res. Atmos. 109. https://doi.org/10.1029/2003JD003635.

French, N.H.F., Hudak, A.T., 2023. Biomass burning fuel consumption and emissions for air quality. In: Landscape Fire, Smoke, and Health. American Geophysical Union (AGU), pp. 69–88. https://doi.org/10.1002/9781119757030.ch5.

Gallacher, J.R., Ripa, B., Butler, B.W., Fletcher, T.H., 2018. Lab-scale observations of flame attachment on slopes with implications for firefighter safety zones. Fire Saf. J. 96, 93–104. https://doi.org/10.1016/j.firesaf.2018.01.002.

Garcia, M., Saatchi, S., Casas, A., Koltunov, A., Ustin, S., Ramirez, C., Garcia-Gutierrez, J., Balzter, H., 2017. Quantifying biomass consumption and carbon release from the California rim fire by integrating airborne LiDAR and landsat OLI data. J. Geophys. Res.: Biogeosciences 122, 340–353. https://doi.org/10.1002/2015JG003315.

Genuer, R., Poggi, J.-M., Tuleau-Malot, C., 2015. VSURF: an R package for variable selection using random forests. The R Journal 7, 19–33.

Gorelick, N., Hancher, M., Dixon, M., Ilyushchenko, S., Thau, D., Moore, R., 2017. Google Earth engine: planetary-Scale geospatial analysis for everyone. Remote Sensing of Environment, Big Remotely Sensed Data: tools, applications and experiences 202, 18–27. https://doi.org/10.1016/j.rse.2017.06.031.

Guerra-Hernández, J., Pereira, J.M.C., Stovall, A., Pascual, A., 2024. Impact of fire severity on forest structure and biomass stocks using NASA GEDI data. Insights from the 2020 and 2021 wildfire season in Spain and Portugal. Science of Remote Sensing 9, 100134. https://doi.org/10.1016/j.srs.2024.100134.

Hancock, S., Armston, J., Hofton, M., Sun, X., Tang, H., Duncanson, L.I., Kellner, J.R., Dubayah, R., 2019. The GEDI simulator: a large-footprint waveform lidar simulator for calibration and validation of spaceborne missions. Earth Space Sci. 6, 294–310. https://doi.org/10.1029/2018EA000506.

Hijmans, R.J., Bivand, R., Pebesma, E., Sumner, M.D., 2023. Terra: Spatial Data Analysis.

Hu, T., Ma, Q., Su, Y., Battles, J.J., Collins, B.M., Stephens, S.L., Kelly, M., Guo, Q., 2019. A simple and integrated approach for fire severity assessment using bi-temporal airborne LiDAR data. Int. J. Appl. Earth Obs. Geoinf. 78, 25–38. https://doi.org/10.1016/j.jag.2019.01.007.

Hudak, A.T., Dickinson, M.B., Bright, B.C., Kremens, R.L., Loudermilk, E.L., O'Brien, J.J., Hornsby, B.S., Ottmar, R.D., 2015. Measurements relating fire radiative energy density and surface fuel consumption – RxCADRE 2011 and 2012. Int. J. Wildland Fire 25, 25–37. https://doi.org/10.1071/WF14159.

Hudak, A.T., Evans, J.S., Stuart Smith, A.M., 2009. LiDAR utility for natural resource managers. Remote Sens. 1, 934–951. https://doi.org/10.3390/rs1040934.

Hudak, A.T., Kato, A., Bright, B.C., Loudermilk, E.L., Hawley, C., Restaino, J.C., Ottmar, R.D., Prata, G.A., Cabo, C., Prichard, S.J., Rowell, E.M., Weise, D.R., 2020. Towards spatially explicit quantification of Pre- and postfire fuels and fuel consumption from traditional and point cloud measurements. For. Sci. 66, 428–442. https://doi.org/10.1093/forsci/fxz085.

Huettermann, S., Jones, S., Soto-Berelov, M., Hislop, S., 2023. Using landsat time series and bi-temporal GEDI to compare spectral and structural vegetation responses after fire. Int. J. Appl. Earth Obs. Geoinf. 122, 103403. https://doi.org/10.1016/j.jag.2023.103403.

Isenburg, M., 2015. Lastools.

Keeley, J.E., 2009. Fire intensity, fire severity and burn severity: a brief review and suggested usage. Int. J. Wildland Fire 18, 116–126. https://doi.org/10.1071/WF07049.

Kennedy, R.E., Yang, Z., Cohen, W.B., 2010. Detecting trends in forest disturbance and recovery using yearly landsat time series: 1. LandTrendr — temporal segmentation algorithms. Rem. Sens. Environ. 114, 2897–2910. https://doi.org/10.1016/j.rse.2010.07.008.

Key, C.H., Benson, N.C., 1999. The normalized burn ratio (NBR): a landsat TM radiometric measure of burn severity. United States Geological Survey, Northern Rocky Mountain Science Center (Bozeman, MT).

Kitchen, S., Behrens, P., Goodrich, S., Green, A., Guyon, J., O'Brien, M., Tart, D., 2019. Guidelines for aspen restoration in Utah with applicability to the intermountain west. General Technical Report RMRS-GTR-390 1–64.

Kobziar, L.N., Lampman, P., Tohidi, A., Kochanski, A.K., Cervantes, A., Hudak, A.T., McCarley, R., Gullett, B., Aurell, J., Moore, R., Vuono, D.C., Christner, B.C., Watts, A. C., Cronan, J., Ottmar, R., 2024. Bacterial emission factors: a foundation for the terrestrial-atmospheric modeling of bacteria aerosolized by wildland fires. Environ. Sci. Technol. 58, 2413–2422. https://doi.org/10.1021/acs.est.3c05142.

Kobziar, L.N., Pingree, M.R.A., Larson, H., Dreaden, T.J., Green, S., Smith, J.A., 2018. Pyroaerobiology: the aerosolization and transport of viable microbial life by wildland fire. Ecosphere 9, e02507. https://doi.org/10.1002/ecs2.2507.

Kolden, C.A., Smith, A.M.S., Abatzoglou, J.T., 2015. Limitations and utilisation of monitoring trends in burn severity products for assessing wildfire severity in the USA. Int. J. Wildland Fire 24, 1023–1028. https://doi.org/10.1071/WF15082.

Kramer, H.A., Collins, B.M., Lake, F.K., Jakubowski, M.K., Stephens, S.L., Kelly, M., 2016. Estimating ladder fuels: a new approach combining field photography with LiDAR. Remote Sens. 8, 766. https://doi.org/10.3390/rs8090766.

Larkin, N.K., Raffuse, S.M., Strand, T.M., 2014. Wildland fire emissions, carbon, and climate: U.S. emissions inventories. Forest ecology and management, wildland fire emissions, carbon, and climate. Science overview and knowledge needs 317, 61–69. https://doi.org/10.1016/j.foreco.2013.09.012.

Leite, R.V., Silva, C.A., Broadbent, E.N., Amaral, C.H. do, Liesenberg, V., Almeida, D.R.A. de, Mohan, M., Godinho, S., Cardil, A., Hamamura, C., Faria, B.L. de, Brancalion, P. H.S., Hirsch, A., Marcatti, G.E., Dalla Corte, A.P., Zambrano, A.M.A., Costa, M.B.T. da, Matricardi, E.A.T., Silva, A.L. da, Goya, L.R.R.Y., Valbuena, R., Mendonça, B.A.F. de, Silva Junior, C.H.L., Aragão, L.E.O.C., García, M., Liang, J., Merrick, T., Hudak, A.T., Xiao, J., Hancock, S., Duncason, L., Ferreira, M.P., Valle, D., Saatchi, S., Klauberg, C., 2022. Large scale multi-layer fuel load characterization in tropical savanna using GEDI spaceborne lidar data. Rem. Sens. Environ. 268, 112764. https://doi.org/10.1016/j.rse.2021.112764.

Lentile, L.B., Morgan, P., Hudak, A.T., Bobbitt, M.J., Lewis, S.A., Smith, A.M.S., Robichaud, P.R., 2007. Post-fire burn severity and vegetation response following eight large wildfires across the Western United States. fire ecol 3, 91–108. https://doi.org/10.4996/fireecology.0301091.

Loehman, R.A., Reinhardt, E., Riley, K.L., 2014. Wildland fire emissions, carbon, and climate: seeing the forest and the trees – a cross-scale assessment of wildfire and carbon dynamics in fire-prone, forested ecosystems. Forest Ecology and Management, Wildland fire emissions, carbon, and climate: Science overview and knowledge needs 317, 9–19. https://doi.org/10.1016/j.foreco.2013.04.014.

Loh, H.Y., James, D., Ioki, K., Wong, W.V.C., Tsuyuki, S., Phua, M.-H., 2022. Estimating aboveground biomass changes in a human-modified tropical montane forest of borneo using multi-temporal airborne LiDAR data. Remote Sens. Appl.: Society and Environment 28, 100821. https://doi.org/10.1016/j.rsase.2022.100821.

Ma, Q., Hu, T., Su, Y., Guo, Q., Battles, J.J., Kelly, M., 2018. Individual tree level forest fire assessment using Bi-temporal LiDAR data. In: IGARSS 2018 - 2018 IEEE International Geoscience and Remote Sensing Symposium. Presented at the IGARSS 2018 - 2018 IEEE International Geoscience and Remote Sensing Symposium, pp. 4308–4311. https://doi.org/10.1109/IGARSS.2018.8519445.

McCarley, T.R., Hudak, A.T., Bright, B.C., Cronan, J., Eagle, P., Ottmar, R.D., Watts, A.C., 2024. Generating fuel consumption maps on prescribed fire experiments from airborne laser scanning. Int. J. Wildland Fire 33. https://doi.org/10.1071/WF23160.

McCarley, T.R., Hudak, A.T., Restaino, J.C., Billmire, M., French, N.H.F., Ottmar, R.D., Hass, B., Zarzana, K., Goulden, T., Volkamer, R., 2022. A comparison of multitemporal airborne laser scanning data and the fuel characteristics classification system for estimating fuel load and consumption. J. Geophys. Res.: Biogeosciences 127, e2021JG006733. https://doi.org/10.1029/2021JG006733.

McCarley, T.R., Hudak, A.T., Sparks, A.M., Vaillant, N.M., Meddens, A.J.H., Trader, L., Mauro, F., Kreitler, J., Boschetti, L., 2020. Estimating wildfire fuel consumption with multitemporal airborne laser scanning data and demonstrating linkage with MODIS-Derived fire radiative energy. Rem. Sens. Environ. 251, 112114. https://doi.org/10.1016/j.rse.2020.112114.

McRoberts, R.E., Næsset, E., Gobakken, T., Bollandsås, O.M., 2015. Indirect and direct estimation of forest biomass change using forest inventory and airborne laser scanning data. Rem. Sens. Environ. 164, 36–42. https://doi.org/10.1016/j.rse.2015.02.018.

Meng, R., Dennison, P.E., Zhao, F., Shendryk, I., Rickert, A., Hanavan, R.P., Cook, B.D., Serbin, S.P., 2018. Mapping canopy defoliation by herbivorous insects at the individual tree level using bi-temporal airborne imaging spectroscopy and LiDAR measurements. Rem. Sens. Environ. 215, 170–183. https://doi.org/10.1016/j.rse.2018.06.008.

Miller, J.D., Knapp, E.E., Key, C.H., Skinner, C.N., Isbell, C.J., Creasy, R.M., Sherlock, J. W., 2009. Calibration and validation of the relative differenced normalized burn ratio (RdNBR) to three measures of fire severity in the sierra Nevada and klamath Mountains, California, USA. Rem. Sens. Environ. 113, 645–656. https://doi.org/10.1016/j.rse.2008.11.009.

Morgan, P., Keane, R.E., Dillon, G.K., Jain, T.B., Hudak, A.T., Karau, E.C., Sikkink, P.G., Holden, Z.A., Strand, E.K., 2014. Challenges of assessing fire and burn severity using field measures, remote sensing and modelling. Int. J. Wildland Fire 23, 1045–1060. https://doi.org/10.1071/WF13058.

Morgan, P., Moy, M., Droske, C.A., Lewis, S.A., Lentile, L.B., Robichaud, P.R., Hudak, A. T., Williams, C.J., 2015. Vegetation response to burn severity, native grass seeding, and salvage logging. fire ecol 11, 31–58. https://doi.org/10.4996/fireecology.1102031.

Mutlu, M., Popescu, S.C., Stripling, C., Spencer, T., 2008. Mapping surface fuel models using lidar and multispectral data fusion for fire behavior. Rem. Sens. Environ. 112, 274–285. https://doi.org/10.1016/j.rse.2007.05.005.

Okyay, U., Telling, J., Glennie, C.L., Dietrich, W.E., 2019. Airborne lidar change detection: an overview of Earth sciences applications. Earth Sci. Rev. 198, 102929. https://doi.org/10.1016/j.earscirev.2019.102929.

Ottmar, R.D., 2014. Wildland fire emissions, carbon, and climate: modeling fuel consumption. Forest Ecology and Management, Wildland fire emissions, carbon, and climate: Science overview and knowledge needs 317, 41–50. https://doi.org/10.1016/j.foreco.2013.06.010.

Page, W.G., Butler, B.W., 2017. An empirically based approach to defining wildland firefighter safety and survival zone separation distances. Int. J. Wildland Fire 26, 655–667.

Pascual, A., Guerra-Hernández, J., 2023. An integrated assessment of carbon emissions from forest fires beyond impacts on aboveground biomass. A showcase using airborne lidar and GEDI data over a megafire in Spain. J. Environ. Manag. 345, 118709. https://doi.org/10.1016/j.jenvman.2023.118709.

Ploton, P., Mortier, F., Réjou-Méchain, M., Barbier, N., Picard, N., Rossi, V., Dormann, C., Cornu, G., Viennois, G., Bayol, N., Lyapustin, A., Gourlet-Fleury, S., Pélissier, R., 2020. Spatial validation reveals poor predictive performance of large-scale ecological mapping models. Nat. Commun. 11, 4540. https://doi.org/10.1038/s41467-020-18321-y.

Price, O.F., Gordon, C.E., 2016. The potential for LiDAR technology to map fire fuel hazard over large areas of Australian forest. J. Environ. Manag. 181, 663–673. https://doi.org/10.1016/j.jenvman.2016.08.042.

Price, O.H., Nolan, R.H., Samson, S.A., 2022. Fuel consumption rates in resprouting eucalypt forest during hazard reduction burns, cultural burns and wildfires. For. Ecol. Manag. 505, 119894. https://doi.org/10.1016/j.foreco.2021.119894.

Prichard, S.J., Kennedy, M.C., Andreu, A.G., Eagle, P.C., French, N.H., Billmire, M., 2019a. Next-generation biomass mapping for regional emissions and carbon inventories: incorporating uncertainty in wildland fuel characterization. J. Geophys. Res.: Biogeosciences 124, 3699–3716. https://doi.org/10.1029/2019JG005083.

Prichard, S.J., Kennedy, M.C., Wright, C.S., Cronan, J.B., Ottmar, R.D., 2017. Predicting forest floor and woody fuel consumption from prescribed burns in southern and Western pine ecosystems of the United States. For. Ecol. Manag. 405, 328–338. https://doi.org/10.1016/j.foreco.2017.09.025.

Prichard, S.J., Larkin, N.S., Ottmar, R., French, N.H.F., Baker, K., Brown, T., Clements, C., Dickinson, M., Hudak, A., Kochanski, A., Linn, R., Liu, Y., Potter, B., Mell, W., Tanzer, D., Urbanski, S., Watts, A., 2019b. The fire and smoke model evaluation experiment—A plan for integrated, large fire–atmosphere field campaigns. Atmosphere 10, 66. https://doi.org/10.3390/atmos10020066.

R Core Team, 2021. R: a Language and Environment for Statistical Computing.

Reinhardt, E.D., Crookston, N.L., 2003. The Fire and Fuels Extension to the Forest Vegetation Simulator. United States Department of Agriculture, Forest Service, Rocky Mountain Research Station.

Restaino, J.C., Peterson, D.L., 2013. Wildfire and fuel treatment effects on forest carbon dynamics in the Western United States. For. Ecol. Manag. 303, 46–60. https://doi.org/10.1016/j.foreco.2013.03.043.

Riccardi, C.L., Ottmar, R.D., Sandberg, D.V., Andreu, A., Elman, E., Kopper, K., Long, J., 2007. The fuelbed: a key element of the fuel characteristic classification SystemThis article is one of a selection of papers published in the special forum on the fuel characteristic classification system. Can. J. For. Res. 37, 2394–2412. https://doi.org/10.1139/X07-143.

Roussel, J.R., Auty, D., Coops, N.C., Tompalski, P., Goodbody, T.R., Meador, A.S., Bourdon, J.F., De Boissieu, Achim, A., 2020. lidR: An R package for analysis of Airborne Laser Scanning (ALS) data. Remote Sens. Environ. 251, 112061.

Roy, D.P., Kashongwe, H.B., Armston, J., 2021. The impact of geolocation uncertainty on GEDI tropical forest canopy height estimation and change monitoring. Science of Remote Sensing 4, 100024. https://doi.org/10.1016/j.srs.2021.100024.

Staley, D.M., Tillery, A.C., Kean, J.W., McGuire, L.A., Pauling, H.E., Rengers, F.K., Smith, J.B., 2018. Estimating post-fire debris-flow hazards prior to wildfire using a statistical analysis of historical distributions of fire severity from remote sensing data. Int. J. Wildland Fire 27, 595–608. https://doi.org/10.1071/WF17122.

Su, Y., Guo, Q., Collins, B.M., Fry, D.L., Hu, T., Kelly, M., 2016. Forest fuel treatment detection using multi-temporal airborne lidar data and high-resolution aerial imagery: a case study in the sierra Nevada Mountains, California. Int. J. Rem. Sens. 37, 3322–3345. https://doi.org/10.1080/01431161.2016.1196842.

Tompalski, P., 2023. Lidrmetrics.

Wallace, L., Hillman, S., Hally, B., Taneja, R., White, A., McGlade, J., 2022. Terrestrial laser scanning: an operational tool for fuel hazard mapping? Fire 5, 85. https://doi.org/10.3390/fire5040085.

Weise, D.R., Wright, C.S., 2014. Wildland fire emissions, carbon and climate: characterizing wildland fuels. Forest Ecology and Management, Wildland fire emissions, carbon, and climate: Science overview and knowledge needs 317, 26–40. https://doi.org/10.1016/j.foreco.2013.02.037.

Wooster, M.J., Roberts, G.J., Giglio, L., Roy, D.P., Freeborn, P.H., Boschetti, L., Justice, C., Ichoku, C., Schroeder, W., Davies, D., Smith, A.M.S., Setzer, A., Csiszar, I., Strydom, T., Frost, P., Zhang, T., Xu, W., de Jong, M.C., Johnston, J.M., Ellison, L., Vadrevu, K., Sparks, A.M., Nguyen, H., McCarty, J., Tanpipat, V., Schmidt, C., San-Miguel-Ayanz, J., 2021. Satellite remote sensing of active fires: history and current status, applications and future requirements. Rem. Sens. Environ. 267, 112694. https://doi.org/10.1016/j.rse.2021.112694.

Wright, M.N., Ziegler, A., 2017. Ranger: a fast implementation of random forests for high dimensional data in C++ and R. J. Stat. Software 77. https://doi.org/10.18637/jss.v077.i01.

Yan, W.Y., 2023. Airborne lidar data artifacts: what we know thus far. IEEE Geoscience and Remote Sensing Magazine 11, 21–45. https://doi.org/10.1109/MGRS.2023.3285261.

Zaragosa, G.P., Paringit, E.C., Ibañez, C.A.G., Faelga, R.A.G., Argamosa, R.J.L., Posilero, M.A.V., Tandoc, F.A.M., Malabanan, M.V., 2016. Addressing lidar overlap for diameter at breast height estimation using a point-cloud processing software, in: Lidar remote sensing for environmental monitoring XV. Presented at the Lidar Remote Sensing for Environmental Monitoring XV, pp. 214–227. https://doi.org/10.1117/12.2223699. SPIE.

Zhang, Jingxiong, Zhang, Jinping, Yao, N., 2009. Uncertainty characterization in remotely sensed land cover information. Geo-Spatial Inf. Sci. 12, 165–171. https://doi.org/10.1007/s11806-009-0072-9.

Zhao, K., Suarez, J.C., Garcia, M., Hu, T., Wang, C., Londo, A., 2018. Utility of multitemporal lidar for forest and carbon monitoring: tree growth, biomass dynamics, and carbon flux. Rem. Sens. Environ. 204, 883–897. https://doi.org/10.1016/j.rse.2017.09.007.

Zhu, Z., Woodcock, C.E., 2014. Continuous change detection and classification of land cover using all available landsat data. Rem. Sens. Environ. 144, 152–171. https://doi.org/10.1016/j.rse.2014.01.011.